Multipartite Non-Locality in Interacting Spin Chains

Salome Hayes-Shuptar

Supervised By Dr. Steve Campbell

UCD School of Physics

This thesis is submitted to University College Dublin in partial fulfilment of the requirements for the degree of BSc in Theoretical Physics

April 27, 2023

Preface

Acknowledgements

The completion of this thesis would not have been possible without the support and participation of numerous people. I would especially like to express my gratitude to my supervisor Dr. Steve Campbell for his enduring patience, guidance and encouragement throughout my undergraduate degree. I would also like to thank the excellent faculty at the UCD School of Physics and my fellow classmates for fostering such a conducive environment for learning.

Declaration of Authorship

I declare that all material in this thesis is my own work, except where there is clear acknowledgement and appropriate reference to the work of others.

Contents

List of Figures

List of Acronyms

EPR	Einstein, Podolsky and Rosen
CHSH	Clauser, Horne, Shimony and Holt
LHV	Local Hidden Variable
MK	Mermin-Klyshko
QMI	Quantum Mutual Information
EF	Entanglement of Formation
GMN	Genuine Multipartite Nonlocality
LOCC	Local Operations and Classical Communication
SLOCC	Stochastic Local Operations and Classical Communication
GHZ	Greenberger-Horne-Zeilinger

Abstract

Recent studies have shown that nonlocality is an important resource in quantum communication and technology for encoding information in physical systems. We aim to investigate how the microscopic description of three spin chain models - XX, Ising and XY - which are used both to characterise real phenomena as well as simulate quantum systems, affects the nonlocality. We discuss various measures of quantum correlations and differentiate them from the definition of nonlocality, which is signified by Bell-like inequalities. In particular, we motivate the use of Svetlichny functions to search for genuine multipartite nonlocality. Thus, we analyse the nonlocal behaviour for 2-spin, 3-spin and 4-spin 1D interacting chains, remarking on the complexity the problem poses to finding analytical solutions. We examine the emergent correlation structures observed and choice of measurement setting needed to optimise the nonlocality at each system size, noting there are two inequivalent correlation structures for 3-particle systems and nine inequivalent structures for 4-particle systems. We observe congruity between the correlation structures and optimal measurement settings for the Ising and XY spin chains in the 3 and 4-particle cases.

Chapter 1

Introduction

We are fortunate to be in the foundational stages of the development of quantum technology. While some fields have already seen practical uses, such as in sensing, cryptography and simulation [1][2][3], the theoretical underpinnings of the subject are still being investigated. Perhaps the two key properties that set quantum mechanics apart from our classical understanding of physics are indeterminacy and nonlocality. The former leads to the unexpected result that "measurement" outcomes are fundamentally probabilistic while the latter derives from the unique correlations that can be found in quantum systems, of which no classical system can replicate. While these correlations can be used as a resource [4], they are fragile, complex and varied, meaning there is no standardised method of quantifying them. Hence it is imperative that we understand their structures and behaviours in order to properly utilise them in quantum technology. The necessity of such research was born out this year, when the 2023 Nobel Prize in Physics was awarded to Alain Aspect, John Clauser and Anton Zeilinger for their pioneering work studying nonlocality.

The concept of nonlocality arose during the formation of quantum theory, when Einstein, Podolsky and Rosen argued that quantum mechanics was an incom-

plete theory because it did not obey what they referred to as "local realism" [5]. Their paper is now referred to as the EPR Paradox. Put simply, locality refers to the condition that events cannot instantaneously affect each other, i.e. they must obey special relativity, while realism refers to the condition that measurement outcomes must be pre-determined, i.e. they must exist whether or not the measurement is performed. To explain this apparent discrepancy there must be some external property not characterised by quantum theory, some "local hidden variable". Attempts were made to explore such hidden variable theories, such as those of Bohmian mechanics or "pilot wave theory" [6], but these were explicitly nonlocal. In 1964, John Bell responded to the EPR paradox when he demonstrated that in fact, no local hidden variable theory can fully reproduce the predictions made by quantum mechanics [7]. Under the assumption of locality, he derived the now famous Bell's inequality composed of correlation functions of measurement outcomes of two particles. Violating the inequality implies violating the assumption of locality, hence "violation of a Bell-like inequality" is considered to be our current signifier of nonlocality. Later on, this inequality was reformulated as the Clauser, Horne, Shimony, and Holt (CHSH) inequality, which lies at the heart of the experiments awarded in the 2023 Physics Nobel Prize.

Although it is clear quantum mechanics does not obey local realism, one might wonder why locality has been disputed to a greater extent than realism in the ensuing decades. Indeed demonstrations such as Young's double slit experiment [8] and its modern variations support the violation of the principle of realism and the existence of superposition in microscopic systems. However, the principle of realism is fundamentally harder to investigate at scale, especially when we have the classical intuition that objects exists even when we are not directly observing them. As Bell himself pointed out, the issue of local realism is not one that can be swept under the rug by adopting the view that quantum mechanics is a

"purely symbolic procedure" [9], as this neglects the very reason we attempt to understand nature [10]. At the same time, such questions like superdeterminism [11] are unanswerable by the scientific method. Hence much of the research in the field has been dedicated to probing the "local" part of "local realism".

Recent investigation has demonstrated the use of nonlocality in communication networks as a tool to encode information in physical systems [12][13]. We are therefore interested in investigating how the quantum picture of these systems manifests in the behaviour of the nonlocality. More specifically we are interested in how the microscopic model, the measurement settings and the system size affect the nonlocality. To investigate the effect of the microscopic description we examine models currently being used to explore quantum phenomena, known as spin chains. They lend themselves to exploring quantum effects as some are fully analytically solvable such as the Ising model [14] and can be experimentally realised [15] [16]. We have already seen their use in quantum communication [17] and while they are often highly simplified models, some do adequately capture the broad strokes of real crystals such as $FeCl_2$ and $FeCO_3$ [18]. Hence investigating these models allows us to explore the correlation structures we observe in physical settings.

To examine the measurement settings, we note that Bell functions are comprised of expectation values of joint measurement outcomes. These are derived by projecting the particles' states onto two observables with measurement outcomes ± 1. As we will define later in the results, these observables can be functions of a complex rotation. We will examine how the nonlocality is affected by the value of the rotation angles, the choice of observable and whether we observe patterns in the maximally violating measurement setting for a specific spin chain.

Finally to investigate system size, we note that due to emergent phenomena at each scale there is no discernible pattern in the number and type of correlation structures for progressively larger systems. The behaviour of nonlocality for even

small system sizes is nontrivial and each case must be examined individually.

1.1 Useful Definitions

As we have motivated the importance of the topic, we now briefly lay out some useful definition. First, a qubit describes the simplest two-level system, with a ground state and excited state. Most commonly in our analysis it will be used to represent whether a particle is in an up spin or down spin configuration, also denoted with 0 and 1,

$$|\uparrow\rangle = |0\rangle = \begin{pmatrix} 1 \\ 0 \end{pmatrix} \qquad |\downarrow\rangle = |1\rangle = \begin{pmatrix} 0 \\ 1 \end{pmatrix} \tag{1.1}$$

The density operator describes the state of a system. If a system is in a pure state, i.e. it cannot be described by a linear combination of states, the trace of the corresponding squared density operator is 1, while if a system is in a mixed state, i.e. some statistical mixture of pure states, the trace of the corresponding squared density operator is strictly less than 1,

$$|\Psi\rangle = \begin{cases} \mathrm{Tr}[\rho^2] = 1 & \text{if pure} \\ \mathrm{Tr}[\rho^2] < 1 & \text{if mixed} \end{cases} \tag{1.2}$$

For a pure state the corresponding density operator can be written as follows,

$$\rho = |\psi\rangle\langle\psi| \tag{1.3}$$

While for a mixed state the density operator is written as a sum over density operators of pure states (sometimes also referred to as an ensemble due to it being

a statistical distribution), where p_i gives the probability of being in state $|\psi_i\rangle$,

$$\rho = \sum_i p_i |\psi_i\rangle\langle\psi_i| \tag{1.4}$$

Separable states are defined as those that can be written as a tensor product, i.e. for a two particle state,

$$|\psi\rangle_{AB} = |\phi\rangle_A \otimes |\varphi\rangle_B \tag{1.5}$$

Sometimes these states are referred to as composite systems, as they are the combination of system A and system B. Following on from this, entangled states are defined as those that cannot be reduced to separable states. An example of entangled states are the Bell states,

$$\begin{aligned} \left|\Phi^+\right\rangle &= \frac{|00\rangle + |11\rangle}{\sqrt{2}} & \left|\Phi^-\right\rangle &= \frac{|00\rangle - |11\rangle}{\sqrt{2}} \\ \left|\Psi^+\right\rangle &= \frac{|01\rangle + |10\rangle}{\sqrt{2}} & \left|\Psi^-\right\rangle &= \frac{|01\rangle - |10\rangle}{\sqrt{2}} \end{aligned} \tag{1.6}$$

Whereas tensor products are used to combine systems, we use the partial trace to consider subsystems. To do this we act with the identity on the subsystem of interest, while summing over the remaining subsystems. For ρ_{AB}, this is defined in Equation 1.7, where $|j\rangle$ is a basis of the subsystem B.

$$\rho_A = \mathrm{Tr}_B\left[\rho_{AB}\right] = \sum_j \left(I_A \otimes \langle j|_B\right) \rho_{AB} \left(I_A \otimes |j\rangle_B\right) \tag{1.7}$$

We denote the von Neumann entropy as $S(\rho)$, as defined in Equation 1.8. When the von Neumann entropy is computed using the partial trace it is referred to as the entanglement entropy, denoted as $S(\rho_A)$ or $E_E(\rho)$.

$$S(\rho) = -\mathrm{Tr}[\rho \ln \rho] \tag{1.8}$$

$$E_E(\rho) = S(\rho_A) = -\mathrm{Tr}[\rho_A \ln \rho_A] \tag{1.9}$$

We will also reference two classes of operations called local operations and classical communication (LOCC) and stochastic local operations and classical communication (SLOCC). LOCC are a family of operators that can only act on one subsystem at a time. SLOCC are a slightly broader family that include measurements with a non-zero probability. Typically these definitions are used in describing various classifications of entanglement in terms of whether a state can be prepared or transformed into another state using only LOCC or SLOCC [19].

Finally, we define the identity operator and the Pauli spin operators as follows,

$$\hat{\mathbb{1}} = \begin{pmatrix} 1 & 0 \\ 0 & 1 \end{pmatrix} \quad \hat{\sigma}_x = \begin{pmatrix} 0 & 1 \\ 1 & 0 \end{pmatrix} \quad \hat{\sigma}_y = \begin{pmatrix} 0 & -i \\ i & 0 \end{pmatrix} \quad \hat{\sigma}_z = \begin{pmatrix} 1 & 0 \\ 0 & -1 \end{pmatrix} \tag{1.10}$$

which correspond to rotations in complex space.

With those definitions established, we lay out the structure of this report. In Section 2 we will outline the mathematical framework underpinning the current definition and computation of nonlocality, known correlation structures and motivate the definitions using the 1D 2-spin Ising chain. In Section 3 we will outline the nonlocality observed in the 2, 3, and 4-spin Ising, XX and XY models. This includes an analytical approach for the 2-spin case and a discussion of universality classes in the 4-spin case. In Section 4 we summarise our analysis and discuss possible future avenues for investigation.

Chapter 2

Theoretical Framework

2.1 Signifiers of Quantum Correlations

As a variety of definitions of quantum correlations exist depending on the system and desired analysis, we will discuss some of the most common methods. In particular, we will compare the definitions used to signify nonlocality with the definitions of correlations and demonstrate they are not equivalent.

Following on from Bell's Theorem [7], the CHSH inequality was devised as it was more amenable to experimental tests [20]. It is one of a class of "Bell-like" inequalities, whose purpose is to verify whether a system obeys locality. We lay out the argument from [5]: consider two quantum experimentalists, Alice and Bob, who are causally disconnected. Suppose that there is some third party that generates pairs of qubits and sends them to Alice and Bob. Call these qubits particle A and particle B respectively. Alice and Bob have each have two measurement settings for their qubit, call them a and a' for qubit A and b and b' for qubit B. The observables a, a', b and b' have outcomes ± 1. Using some method for random selection, Alice and Bob choose a setting and perform a measurement on their qubit, recording the outcome. This process is then repeated, allowing us to

generate a relationship between the expectation values of the operators as follows,

$$|\langle ab\rangle + \langle a'b\rangle + \langle a'b'\rangle - \langle ab'\rangle| \leq 2 \tag{2.1}$$

Where the quantities $\langle\cdot\rangle$ are referred to as correlation functions. We can indeed verify that Equation 2.1 is valid by examining the quantity $E = ab+a'b-ab'+a'b'$. Factorising the expression we get $(a + a')b + (a' - a)b'$. Hence the possible values of E based on the possible combinations of a and a' are, remembering $b = \pm 1$,

$$E = \begin{cases} a = a' = 1 & \implies E = \{-2, 2\} \\ a = a' = -1 & \implies E = \{2, -2\} \\ a = -1,\ a' = 1 & \implies E = \{-2, 2\} \\ a = 1,\ a' = -1 & \implies E = \{2, -2\} \end{cases} \tag{2.2}$$

Either of the two $(a + a')$ or $(a' - a)$ is always zero while the other is 2 or -2. Assuming the probability of qubit A and qubit B of being in definite states before measurement is $\sum_{a,a',b,b'} p(a, a', b, b') = 1$ we find the expectation value of this expression is upper bounded by 2,

$$\begin{aligned} \langle ab + a'b - ab' + a'b'\rangle &= \sum_{a,a',b,b'} p(a, a', b, b')(ab + a'b - ab' + a'b') \\ &\leq \sum_{a,a',b,b'} p(a, a', b, b') \cdot 2 \leq 2 \end{aligned} \tag{2.3}$$

Using the property that the expectation value is linear, we find Equation 2.1. However, what would happen if we considered the third party sending Alice and Bob qubits decided to prepare two qubits in the Bell state $|\Psi^-\rangle$? Alice and Bob now perform the following measurements on their qubits,

$$a = \hat{\sigma}_z \qquad a' = \hat{\sigma}_x \qquad b = -\frac{\hat{\sigma}_z + \hat{\sigma}_x}{\sqrt{2}} \qquad b' = \frac{\hat{\sigma}_z - \hat{\sigma}_x}{\sqrt{2}} \tag{2.4}$$

And if we compute the correlation functions in Equation 2.1 using these new observables, i.e. $\langle ab\rangle = \langle\Psi^-|ab|\Psi^-\rangle$, we find the following values,

$$\begin{gathered}\langle ab\rangle = \frac{1}{\sqrt{2}} \qquad \langle a'b\rangle = \frac{1}{\sqrt{2}} \qquad \langle a'b'\rangle = \frac{1}{\sqrt{2}} \qquad \langle ab'\rangle = -\frac{1}{\sqrt{2}} \\ \implies \langle ab\rangle + \langle a'b\rangle + \langle a'b'\rangle - \langle ab'\rangle = 2\sqrt{2}\end{gathered} \tag{2.5}$$

Hence we see that this entangled Bell state violates the CHSH inequality. This unexpected result can be explained by either of the to two assumptions we made. First, we assumed the qubits A and B must be in definite states before the measurement and second, we assumed a measurement on qubit A does not have influence on the measurement outcome of qubit B. For reasons discussed in Chapter 1, we take the violation to indicate a state must be nonlocal, as opposed to not real, and we refer to it as a *violation*. The CHSH inequality in particular is a method to test for *bipartite* nonlocality.

It has also been used in experimental demonstration [21][22] of Bell's inequality with photons and polarisers, as shown in Figure 2.1. The experiment goes as follows: a source at S emits two spin-$\frac{1}{2}$ photons in a singlet state in opposite directions to polarisers a and b, where the polarisation angle can be chosen by the experimentalist. The ideal "Bell test angles" which give maximal violation are $a = 0$, $a' = \frac{\pi}{2}$, $b = \frac{\pi}{4}$ and $b' = \frac{3\pi}{4}$ [21], which correspond to two rotation observables per particle. The polarisers serve to measure the spin components of the photons along

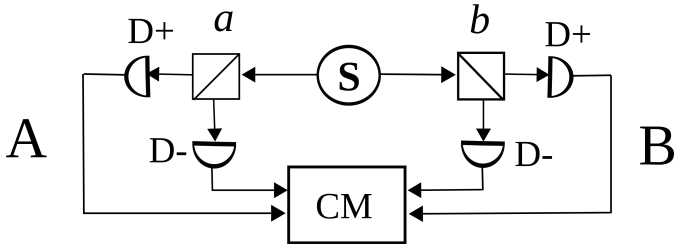

Figure 2.1: Apparatus for 2 particle Bell test, where S is a source for spin-$\frac{1}{2}$ photons in a singlet state, (a, b) correspond to polarisers set to an angle at the experimentalist's discretion, D^+ and D^- are photomultipliers to detect the photons and CM counts the coincidences of measurement outcomes.

orientations $\vec{a}$ and $\vec{b}$. If the resulting photon is parallel to $\vec{a}$ it is detected at the D^+ photomultiplier and counted as a $+1$ outcome, while if it is perpendicular to $\vec{a}$ it is detected at the D^- photomultiplier and counted as a -1 outcome. Similarly for the photon passing through the b or b' polariser. The coincidences are then counted for that configuration of $\langle ab \rangle$, allowing their expectation value to be computed. The process is then repeated for every combination of outputs as defined in the CHSH inequality.

While this experiment, conducted by John F. Clauser [22], did confirm quantum theory's nonlocal nature for some, there were initially still doubts as to its veracity and many classical explanations or "loopholes" were leveled against it. These include the detection loophole [23], the locality loophole [24], the coincidence loophole [25] and the memory loophole [26]. Briefly, the detection loophole argued that the apparatus was not sensitive enough and a more accurate detector would obey the Bell test. The locality loophole argued that if the qubits are timelike separated, the choice of initial measurement setting for one qubit could affect the other qubit's outcomes via classical signals. The coincidence loophole argued that for experiments relying on photon being detected within close enough time intervals to verify whether they were generated together, local hidden variables could be delaying detection times and hence skewing the resulting statistics. Finally the memory loophole argued that since most experiments repeat the measurements at the same physical locations, a local hidden variable could exploit its "memory" of past settings and outcomes. All these loopholes have been addressed separately or in some combination [21] [27], resulting in a few supposedly "loophole-free" experiment in 2015 [28][29][30].

While the CHSH inequality is only defined for bipartite systems, there do exist Bell-like inequalities for more particles. Looking at tripartite states, Svetlichny conceptualised the idea of "genuine multipartite nonlocality" (GMN) [31]. He

identified the need to derive tests of nonlocality specifically for many body systems, as each new system size has its own unique correlation structures due to emergent behaviours. In order to satisfy the definition of GMN, it is necessary that a tripartite state is not separable into a nonlocally correlated bipartite state with a locally correlated state, which would be written as follows,

$$p(abc) = \int q(ab|\lambda) r(c|\lambda) d\rho(\lambda) \tag{2.6}$$

where $p(abc)$ represents the joint probability of particles 1, 2 and 3 being in states with outcomes a, b and c. Here λ represents a local hidden variable (LHV), which determines the outcomes of the measurements on particles 1, 2 and 3 with a probability of $d\rho(\lambda)$. Hence, the probabilities of particles 1 and 2 having outcomes ab after a measurement, given a LHV of λ, is $q(ab|\lambda)$, while the probability of particle 3 having an outcome of c, given a LHV of λ, is $r(c|\lambda)$.

For three qubits, A, B and C, with measurement outcomes (a, a'), (b, b') and (c, c'), Svetlichny's inequality (suitably normalised to one) for tripartite states can be defined as follows [31],

$$\langle abc\rangle + \langle ab'c'\rangle + \langle a'bc\rangle + \langle a'b'c\rangle - \langle a'bc\rangle - \langle ab'c\rangle - \langle abc'\rangle - \langle a'b'c'\rangle \leq 1 \tag{2.7}$$

Using Mermin-Klyshko (MK) polynomials [32], it is possible to extend this definition of nonlocality to n-body Bell-like inequalities for larger systems. These generalised inequalities form the basis for our analysis as they are not satisfied by bipartite nonlocality and hence verify GMN. Consider n qubits labeled $\{A, B, C, D...\}$ with measurement outcomes of $\{(a, a'), (b, b'), (c, c')...\}$ for each particle. Denoting some arbitrary qubit as X with measurement outcomes (x, x'), the MK polynomi-

als can by expressed as follows,

$$\begin{aligned} m_n &= \frac{1}{2} m_{n-1}(x_n + x'_n) + \frac{1}{2} M_{n-1}(x_n - x'_n) \\ M_n &= \frac{1}{2} M_{n-1}(x_n + x'_n) + \frac{1}{2} m_{n-1}(x'_n - x_n) \end{aligned} \tag{2.8}$$

where $m_1 = x_1$ and $M_1 = x'_1$. Note that for each new particle, two new observables, (x_n, x'_n), must be defined. The generalised Svetlichny polynomials can thus be written as [33],

$$S_n = \begin{cases} m_n & \text{(n even)} \\ (m_n + M_n)/2 & \text{(n odd)} \end{cases} \tag{2.9}$$

where S_n can also be referred to as the Svetlichny function. For systems obeying local realism, S_n imposes an upper bound of one, while for nonlocal systems, S_n reaches a maximal violation of $\sqrt{2^{n-1}}$ or $\sqrt{2^{n-2}}$, for the even or odd cases respectively.

Turning away from nonlocality for a moment; mutual information is a measure of the correlations between random variables. Its quantum counterpart, quantum mutual information (QMI), captures both quantum and classical correlations. The QMI between two systems A and B, denoted by $I(A : B)$, is defined in terms of the von Neumann Entropy from Equation 1.8,

$$I(A : B) = S(\rho^A) + S(\rho^B) - S(\rho^{AB}) \tag{2.10}$$

We note the fact that the decomposition of an ensemble in terms of pure states is not unique. Hence we define the entanglement of formation (EF) as a natural extension of the entanglement entropy for mixed states. To compute the EF we minimise the entanglement entropy of all the pure state decompositions of the

mixed state [34],

$$E_F(\rho) = \min \sum_i p_i E_E(|\psi_i\rangle) \tag{2.11}$$

where $|\psi_i\rangle$ are the pure states in the decomposition of ρ, as given in Equation 1.4. Equivalently, the EF can be defined in terms of a quantity known as concurrence. Concurrence was initially defined for two particles, utilising the fact that for pure entangled states such as a Bell state, the reduced density operators of the subsystems are not pure. This definition was later extended to higher dimensions, as follows [35],

$$C\left(\rho_{AB}\right) = \sqrt{2(1 - \mathrm{Tr}\left(\rho_A^2\right))} \tag{2.12}$$

We can write the EF in terms of C as follows, where $h(x)$ is defined as the Shannon entropy function [36],

$$\begin{aligned} E_F(\rho) &= h\left(\frac{1+\sqrt{1-C(\rho)^2}}{2}\right) \\ h(x) &= -x\log_2 x - (1-x)\log_2(1-x) \end{aligned} \tag{2.13}$$

The QMI, EF and Bell-like inequalities give three differing methods to signify, and sometimes quantify, correlations in a quantum systems. Note that the magnitudes of these three quantities are not necessarily comparable, rather it is *when* we observe non-zero values for all three that is of note.

With these definitions in hand, we can compare them using a 2-qubit Werner state [37], which is a bipartite quantum state defined by one parameter, p, which determines the weighting of the subsystems. The 2-qubit Werner state can be written as follows, where $|\Phi^+\rangle$ is the Bell-state defined in Equation 1.6,

$$\varrho_x = \frac{1-p}{4}\hat{\mathbb{1}} + p|\Phi^+\rangle\langle\Phi^+| \tag{2.14}$$

The procedure for computing the CHSH violation is as follows. We begin by

choosing a measurement setting, $\hat{R}(\theta)$, which determines the rotation performed on each spin in complex space. We want two measurement outcomes associated with each spin. Following the notation established in Equation 2.1, the measurement settings a and a' would be $\hat{R}(\theta)$ and $\hat{R}(\theta')$ respectively. Similarly we have $\hat{R}(\phi)$ and $\hat{R}(\phi')$ corresponding to measurements b and b'. The equivalent correlation function to $\langle ab \rangle$ is then expressed as Equation 2.16.

$$\hat{R}(\theta) = \begin{pmatrix} \cos\theta & -i\sin\theta \\ i\sin\theta & -\cos\theta \end{pmatrix} \tag{2.15}$$

$$\langle \hat{R}(\theta_i)\hat{R}(\phi_i) \rangle = \mathrm{Tr}[\hat{R}(\theta_i) \otimes \hat{R}(\phi_i)\varrho_x] \tag{2.16}$$

We can then write the CHSH function in terms of these observables as follows,

$$S_2 = \frac{1}{2}\Big(\langle \hat{R}(\theta)\hat{R}(\phi) \rangle + \langle \hat{R}(\theta')\hat{R}(\phi) \rangle + \langle \hat{R}(\theta')\hat{R}(\phi') \rangle - \langle \hat{R}(\theta)\hat{R}(\phi') \rangle \Big) \tag{2.17}$$

This allows us to write the CHSH function for the 2-qubit Werner state as defined in Equation 2.17. We find that for $p > \frac{1}{\sqrt{2}}$, the Werner state violates the CHSH inequality.

$$\mathrm{CHSH}_{\mathrm{Werner}} = \sqrt{2}p \tag{2.18}$$

To compute the QMI, we take the partial trace of ϱ_x over each subsystem and find in this case they are equivalent. We then use these density matrices in conjunction with the entanglement entropy from Equation 1.9, and von Neumann entropy from Equation 1.8, to find an analytical expression for the QMI of the 2-qubit Werner state, given in Appendix A.

$$\varrho_1 = \varrho_2 = \begin{pmatrix} \frac{1}{2} & 0 \\ 0 & \frac{1}{2} \end{pmatrix} \qquad \mathrm{QMI}_{\mathrm{Werner}} = S(\varrho_1) + S(\varrho_2) - S(\varrho) \tag{2.19}$$

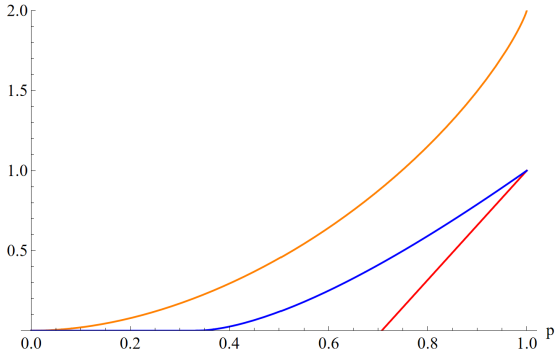

Figure 2.2: QMI (Orange), EF (Blue) and CHSH Violation (Red) for a 2-qubit Werner state as a function of the mixing parameter, p. The QMI is nonzero for any value of p, while the EF is only nonzero for $p \geq \frac{1}{3}$ and the CHSH violation is the most stringent signifier of correlation. At maximal entanglement, $p = 1$, the EF is exactly half of the QMI, while the magnitude of the CHSH violation has been normalised to 1, as the only relevant information is the value of p at which it begins violating.

The EF in terms of the concurrence, computed from Equation 2.13 for $p \geq \frac{1}{3}$, is also given in Appendix B. It is precisely zero for $p < \frac{1}{3}$. The resulting CHSH violation, QMI and EF are plotted against parameter p in Figure 2.2. When $p = 0$ the state is completely separable and for $p \geq \frac{1}{3}$ the state is entangled. At $p = 1$ the state becomes maximally entangled.

It is clear that entanglement and nonlocality are different concepts. For any non-zero value of p there are classical correlations as shown by the QMI, while only beyond some critical value, $p \geq \frac{1}{3}$, when the Werner state becomes entangled, does the EF become non-zero. Finally, the strictest requirement of correlation is the CHSH violation, which only becomes non-zero for a much larger value of p. In other words, states can be entangled but *not* necessarily nonlocal [37].

2.2 Correlation Structures

As mentioned in the previous section, Svetlichny inequalities provide a means to signify GMN. We specifically define GMN between three or more particles because for two particles, correlations either do or do not exist. However, the situation changes for three or more particles as we begin to see different correlation struc-

tures. In fact, it was found that for tripartite systems there are precisely two types of GMN structures. All other forms of tripartite systems can be classified into these two categories, as it is not possible to convert between the two structures via LOCC alone [38]. These are known as the W state and the Greenberger-Horne-Zeilinger (GHZ) state [39]. The GHZ state is known as *"maximally entangled"* while the W state is *"maximally robust"* [38]. These expressions refer to the fact that the GHZ state possesses the highest violation found in tripartite states, while the W state leaves behind the maximally bipartite entangled state upon tracing out one particle. The tripartite W and GHZ states can be written as follows,

$$|W\rangle = \frac{|100\rangle + |010\rangle + |001\rangle}{\sqrt{3}} \tag{2.20}$$

$$|GHZ\rangle = \frac{|000\rangle + |111\rangle}{\sqrt{2}} \tag{2.21}$$

These states represent two fundamentally different types of correlation structures. We can illustrate their difference by imagining the remaining correlations in a tripartite system after removing a particle, as depicted in Figure 2.3. In Figure 2.3a, the ϕ and θ particles remain correlated after tracing out ψ, whereas in Figure

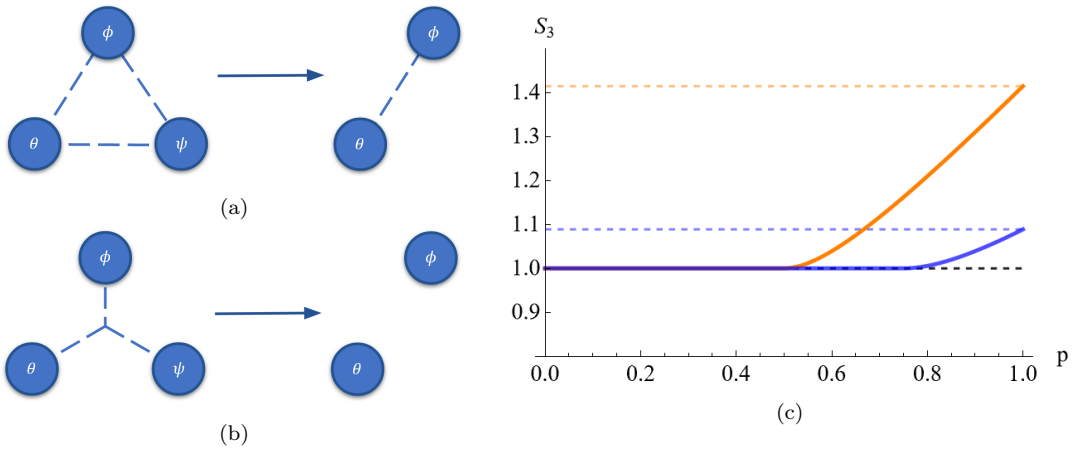

Figure 2.3: **(a)** Diagrammatic representation of the W-type correlation structure **(b)** Diagrammatic representation of the GHZ-type correlation structure **(c)** Svetlichny violation of the tripartite GHZ state (orange) and W state (blue). GHZ state reaches maximal violation at $\sqrt{2}$ while the W state reaches maximal violation S_W^*.

2.3b, ϕ and θ are completely uncorrelated after tracing out ψ. Hence the W state is a more robust but less nonlocal form of correlation while the GHZ represents a fragile but more nonlocal form.

We can compare the Svetlichny violation between these two correlation structures, as shown in Figure 2.3c, using the state:

$$\varrho = \frac{1-p}{8}\hat{I} + p|\psi_X\rangle\langle\psi_X| \qquad X = W \text{ or } X = GHZ \tag{2.22}$$

We see that the GHZ violation, represented by the orange curve, reaches the maximal value of $\sqrt{2}$ for a pure state $p = 1$, while the W violation, represented by the blue curve, reaches a maximal violation of $\simeq 1.1$, call it S_W^*, when $p = 1$. Hence for this measurement setting, any violation $S_W^* \leq S_3 \leq \sqrt{2}$ indicates the state is a GHZ state, while any violation $S_3 \leq S_W^*$ could be either correlation type.

2.3 1D Ising Model

We now consolidate this framework by examining the 1D Ising model, comparing our results against previous literature [33]. We define the Hamiltonian for a 1D chain of spins with periodic boundary conditions such that the $n = N + 1$ spin is equivalent to the $n = 1$ spin as follows,

$$H = \sum_{i=1}^{N} \sigma_x^i \otimes \sigma_x^{i+1} - b\sum_{i=1}^{N} \sigma_z^i \tag{2.23}$$

where the first term describes nearest-neighbour interactions and b characterises the ratio of magnetic field strength to coupling constant. We will analyse both the zero temperature and finite temperature limits for up to 7 spins and up to 4 spins respectively. To begin the analysis we examine the energy spectrum of the 2-spin Ising chain, as shown in Figure 2.4a.

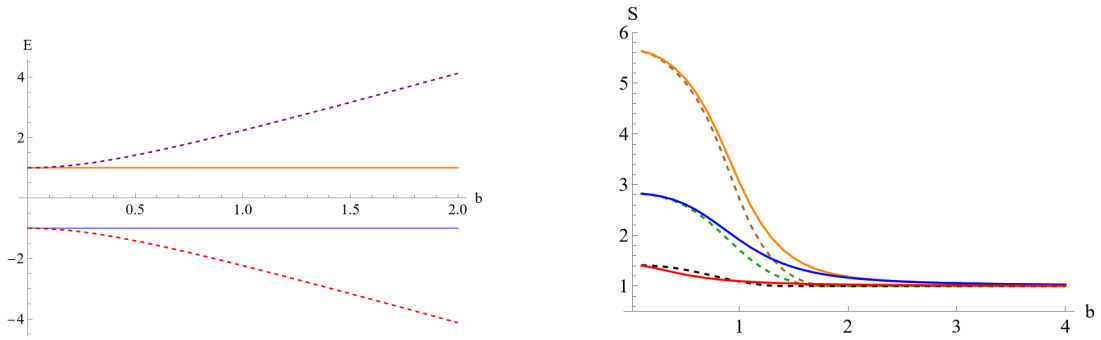

(a) (b)

Figure 2.4: **(a)** Energy spectrum for a 2-spin Ising chain as a function of magnetic field strength. Plotted are the ground state (red, dashed), first excited state (blue, solid), second excited state (orange, solid) and third excited state (purple, dashed) **(b)** Svetlichny violation for the ground state Ising chain for 2 spins (red, solid), 3 spins (black, dashed), 4 spins (blue, solid), 5 spins (green, dashed), 6 spins (orange, solid) and 7 spins (brown, dashed).

The ground state associated with Figure 2.4a can be written as follows, as a function of b,

$$|\Psi_{GS}\rangle = -\left(\sqrt{4b^2+1}+2b\right)|00\rangle + |11\rangle \tag{2.24}$$

This is a highly correlated state, which becomes the familiar Bell state $|\Phi^-\rangle$ in the limit as $b \to 0$. However when b is precisely 0, the ground state becomes a superposition between the degenerate states which is a separable and hence uncorrelated state,

$$|\Psi_{GS}\rangle_{b=0} = \frac{1}{2}\Big(|11\rangle + |10\rangle - |01\rangle - |00\rangle\Big) = \frac{1}{2}\Big(|1\rangle - |0\rangle\Big)\Big(|0\rangle + |1\rangle\Big) \tag{2.25}$$

It is only in the limit as $b \to 0$ that the 2-spin zero temperature Ising chain attains the maximal CHSH violation of $\sqrt{2}$. Away from $b = 0$, the ground state favours the $|00\rangle$ state, which explains why the violation decreases for increasing b. We plot the CHSH and Svetlichny functions in Figure 2.4b, where the solid red curve indicates the 2-spin case. As expected, the CHSH violation attains a maximal violation of $\sqrt{2}$ in the limit as $b \to 0$ and asymptotically tends towards 1. This corresponds to the $|00\rangle$ state dominating and the $|11\rangle$ contribution being negligible, where $|00\rangle$ corresponds to a separable non-violating state.

We have also plotted the Svetlichny functions for $3 \leq n \leq 7$ in Figure 2.4b, where the dotted curves correspond to odd system sizes and the solid curves correspond to even system sizes. Similar behaviour to the 2-spin case can be observed, where the maximal violation is achieved in the limit as $b \to 0$ and the asymptotic limit is $S_n = 1$. While the same maximal bound of the Svetlichny function is achieved for pairs of system sizes (i.e. $n = 2$ and $n = 3$ share the same upper bound) the precise behaviour as a function of b is not equivalent. The 3-spin case seems to violate more for a slightly larger value of b as compared to the 2-spin case, whereas for the $n = (4, 5)$ and $n = (6, 7)$ pairs, the odd system has a violation less than or equal to the even system.

Lastly we will examine the thermalised Ising chain to explore the effect finite temperature would have on nonlocality. While our analysis will primarily examine the ground states of our spin chains of interest, the finite temperature behaviour of the Ising and XX model are known [33] [40]. We proceed by defining the thermal state in Equation 2.26, where $\beta = \frac{1}{k_B T}$. For our analysis we use natural units, setting $k_B = 1$.

$$\rho = \frac{e^{-\beta H}}{\sum_i e^{-\beta E_i}} \tag{2.26}$$

As shown in Figure 2.5, the maximal violation obtained in both the $n = 2$ and $n = 3$ case is $\sqrt{2}$, while it reaches $2\sqrt{2}$ for $n = 4$ as expected. For each value of b, the highest violation obtained is in the limit as $T \to 0$ for the ground state. This is due to the ground state being the only pure state. We observe that increasing the temperature for all cases causes a reduction in the violation, due to the finite temperature mixing the state, and this reduction eventually dips below the local bound of one. However, as we increase the magnetic field strength, the temperature at which the state no longer violates the Svetlichny inequality also increases. In other words, the state can withstand greater thermal mixing the larger the magnetic field is. We understand this as the magnetic field aligning the

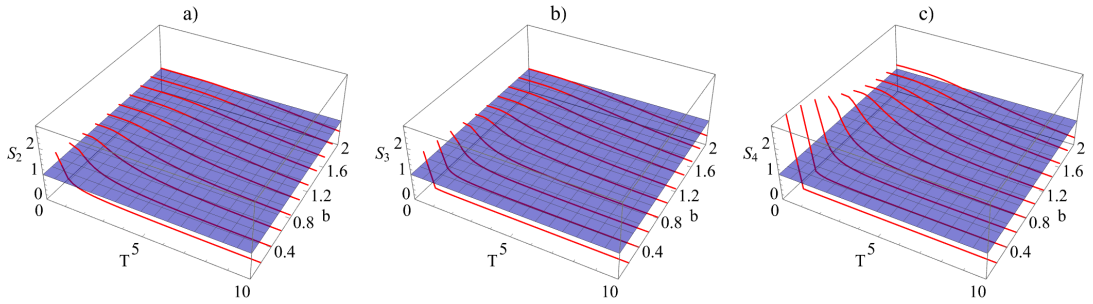

Figure 2.5: For each plot the blue plane indicates the local bound of one. When the Svetlichny function is above this bound, we have a violation. Plotted are the Svetlichny functions of the Ising chain thermal state against temperature and magnetic field strength for **(a)** 2 spins, **(b)** 3 spins and **(c)** 4 spins.

spins, increasing the correlations between them and their resistance to thermal fluctuations. On the other hand, for values of b in the neighbourhood of zero, the degeneracy in the ground state is just barely broken, such that the ground state and first excited state energy levels are very close. This results in strong correlations between the two states, which explains the overall higher violation obtained for smaller values of b. Hence there is a trade off in the magnetic field strength - for low b, the gap in the spectra between the ground state and excited states is small enough for correlations to still exist, while for large b, the spins become increasingly aligned.

However, we know that the ground state 1D Ising model is simply a GHZ-type state for any system size. We are now interested in exploring whether other spin chain models can access different GMN structures we know to exist. Hence, in conjunction with the Ising model, we now examine both the XX and XY models for 2, 3 and 4-particle system sizes.

Chapter 3

Results

3.1 2 Particles

First we define a general Hamiltonian encompassing the XX, XY and Ising models as follows,

$$H = \frac{1+\gamma}{2}\sum_{i=1}^{N}\sigma_x^i \otimes \sigma_x^{i+1} + \frac{1-\gamma}{2}\sum_{i=1}^{N}\sigma_y^i \otimes \sigma_y^{i+1} + \Delta\sum_{i=1}^{N}\sigma_z^i \otimes \sigma_z^{i+1} - b\sum_{i=1}^{N}\sigma_z^i \quad (3.1)$$

where γ is an anisotropy parameter determining how aligned the spins are, Δ determines whether there are spin interactions along the same axis as the external magnetic field, and b is the ratio of the magnetic field strength to spin coupling. When $0 < \gamma < 1$, the Hamiltonian describes the XY model, when $\gamma = 1$, it describes the Ising model and when $\gamma = 0$, it describes the XX model.

For the $n = 2$ case, the Hamiltonian simplifies to,

$$H_2 = \frac{1+\gamma}{2}(\sigma_x^1 \otimes \sigma_x^2) + \frac{1-\gamma}{2}(\sigma_y^1 \otimes \sigma_y^2) - b(\sigma_z^1 \otimes \hat{I} + \hat{I} \otimes \sigma_z^2) \quad (3.2)$$

In the Ising limit, this generates the known behaviour as discussed in Section

2.3. In addition to replicating those results, we attempted to derive an analytical expression for the CHSH violation by examining the behaviour of the rotation angles in the measurement settings. It is clear from Equation 2.17 that the CHSH violation is a function of the angles $(\theta_1, \theta_2, \phi_1, \phi_2)$ where θ_i corresponds to the two measurement settings on spin 1 and ϕ_i corresponds to the two measurement settings on spin 2. If we observe regions where the angles are well-behaved, we can reduce the degrees of freedom in this optimisation problem, allowing us to potentially derive an analytical approximation of the CHSH inequality for a 2-spin Ising chain.

For this portion of the analysis, we use the same measurement setting defined for the Werner state, Equation 2.15. The values of the angles were computed numerically as a function of b, and certain combinations of their sums and differences were plotted, as shown in Figure 3.1. Two distinct regions emerge where $(\theta_1 - \theta_2)$, $(\phi_1 - \phi_2)$, $(\theta_2 + \phi_2)$ and $(\theta_2 - \phi_2)$ are approximately constant. We denote the range $b \in [0, 0.55]$ as region 1 and $b \in [0.65, 1]$ as region 2. We opted not to derive an analytical approximation for the region $b \in [0.56, 0.64]$ as the behaviour is not as

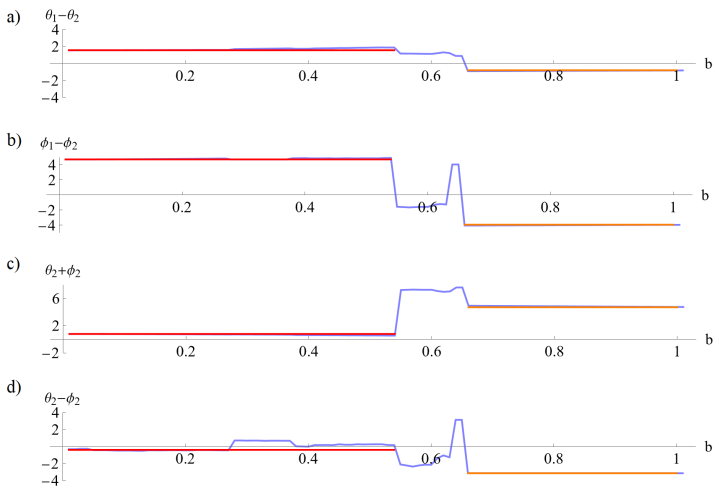

Figure 3.1: For each figure the numerical results of the angle values are plotted in blue, the analytical estimate in region one is plotted in red and the analytical estimate in region two is plotted in orange as a function of b **(a)** Plot of numerical values of $\theta_1 - \theta_2$ **(b)** Plot of numerical values of $\phi_1 - \phi_2$ **(c)** Plot of numerical values of $\theta_2 + \phi_2$ **(d)** Plot of numerical values of $\theta_2 - \phi_2$.

consistent.

The approximations made for each region are given in Appendix C, where the errors of the estimates with respect to the numerical values are one the order of 10^{-3} in region 1 and 10^{-2} in region 2. Similarly, the general analytical expression for the CHSH inequality of the 2-spin Ising chain as a function of $(b, g, \theta_1, \theta_2, \phi_1, \phi_2)$ is given in Appendix D. We substitute these estimates for the angles into the general CHSH expression, which gives us two functions corresponding to the two regions we identified,

$$\text{CHSH}_1 = \frac{\sqrt{2}b^2 + \sqrt{4b^2+1} + 1/\sqrt{8}}{2b^2 + 0.5} \quad \text{CHSH}_2 = 0.957107 + \frac{1}{4\sqrt{4b^2+1}} \tag{3.3}$$

We plot these functions alongside the numerically derived CHSH violation, S_2, as well as the error of the analytical expressions, ΔS_2 in Figure 3.2b. We see for $b \leq 0.3$ the analytical approximation has an error on the order of 10^{-6}. However this error quickly grows for $b > 0.3$ and in particular, the analytical expression for region 2 does not overlap with the numerical CHSH violation at all. We conclude that the observed nonlocality is relatively sensitive to small fluctuations in the values of the rotation angles, making the task of analytically deriving the expression of the CHSH inequality nontrivial.

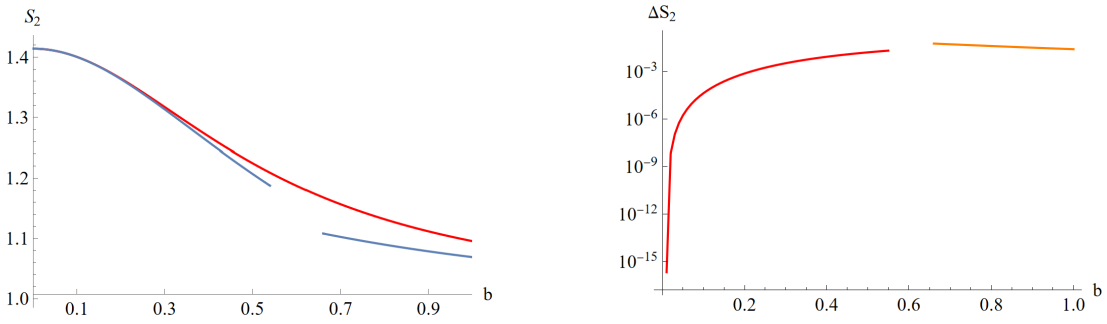

(a) (b)

Figure 3.2: **(a)** Plot comparing the numerical Svetlichny function (red) against the analytical approximations for region one and region two (blue) **(b)** Plot showing the error on the analytical estimate for region one (red) and region two (orange).

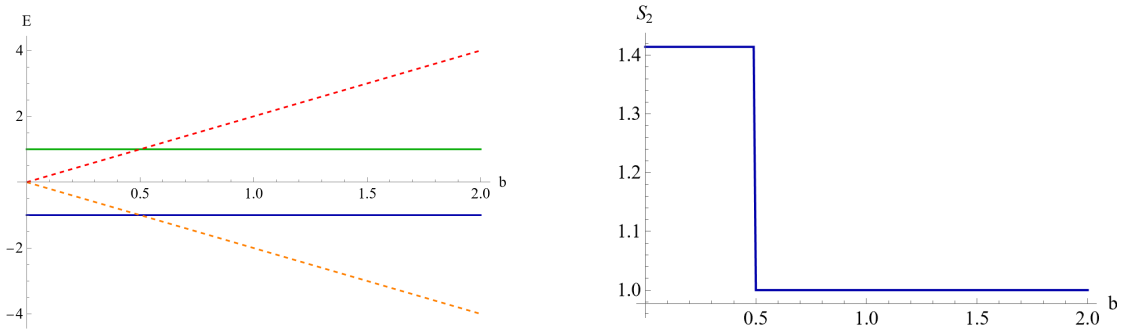

(a) (b)

Figure 3.3: **(a)** Energy spectrum for a 2-spin XX chain as a function of magnetic field strength. Plotted is the ground state before the energy level crossing at $b = 0.5$ (blue, solid) and after the energy level crossing (orange, dotted), and the excited energies **(b)** CHSH function for the ground state XX chain where the discontinuity at $b = 0.5$ corresponds to the energy level crossing.

We next analysed the XX model limit, where $\gamma = 0$. The energy spectrum of the XX model displays a degeneracy of the first excited state at precisely $b = 0$ and an energy level crossing in the ground state at $b = 0.5$. The analytical expression of the ground state can be written as follows,

$$|\Psi_{GS}^{\mathrm{XX}}\rangle = \begin{cases} \frac{1}{\sqrt{2}}\left(|10\rangle - |01\rangle\right) & b \leq 0.5 \\ |00\rangle & b > 0.5 \end{cases} \tag{3.4}$$

Before the energy crossing the ground state is the familiar Bell state, $|\Psi^-\rangle$, which is a highly correlated state. In this region the XX model attains maximal violation of the CHSH function. After the energy crossing the ground state is the separable state $|00\rangle$, which is completely uncorrelated and hence displays no violation, as seen in Figure 3.3b. We also perform an analytical analysis of the 2-spin XX model. This case is relatively simple as the CHSH violation is constant both before and after the energy crossing. Using the same measurement setting as for the analysis of the Werner state and Ising limit, Equation 2.15, we can find exact values of the angles that optimise the inequality, given in Appendix E.

For the last 2-spin chain, we analyse the XY model where $\gamma \in (0, 1)$ for varying b and γ. The XY model also displays energy level crossings in its energy spectra, as

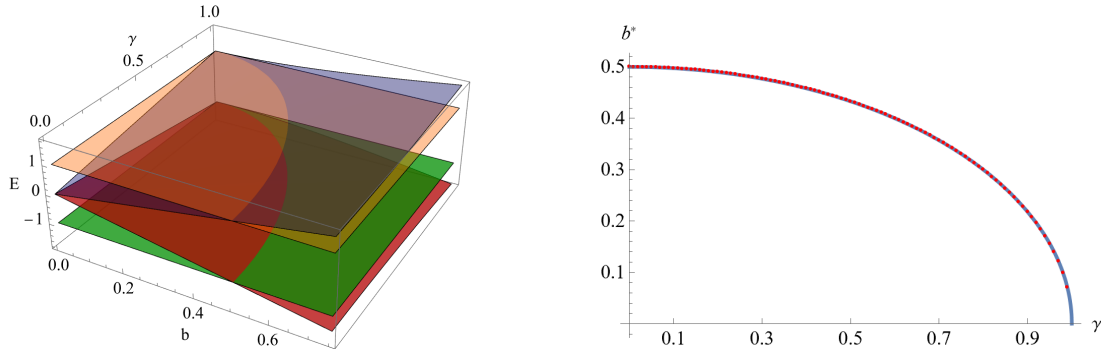

(a) (b)

Figure 3.4: **(a)** Energy spectra of the 2-spin XY chain. There is an energy level crossing beginning at $b^* = 0.5$ in the XX limit and ending at $b^* = 0$ in the Ising limit **(b)** Plot of the numerical values of b^* where the energy level crossing occurs (red, dotted) against the analytical expression (blue, solid).

seen in Figure 3.4a. We also derived the analytical expression for the critical value of b at which the energy level crossing occurs, denoted as b^*, in Equation 3.5. Our analytical expression for b^* is plotted in blue with the numerical values plotted in red, as shown in Figure 3.4b.

$$b^* = \frac{\sqrt{1-\gamma^2}}{2} \tag{3.5}$$

For analysing the CHSH violation of the XY model, we compared the results between three different measurement settings to assess how robust the correlations are to changes in these settings. Note that any measurement setting used specifically in a Bell-like inequality must satisfy two conditions; first, it must have precisely two outcomes and second, those outcomes must be ± 1. The measurement settings used are as follows, where $\hat{R}^3$ is equivalent to the measurement setting used in the analysis of the Werner, W, GHZ, 2-spin Ising and 2-spin XX states.

$$\hat{R}^1 = \cos\theta\hat{\sigma}_x + \sin\theta\hat{\sigma}_y \quad \hat{R}^2 = \cos\theta\hat{\sigma}_x + \sin\theta\hat{\sigma}_z \quad \hat{R}^3 = \cos\theta\hat{\sigma}_z + \sin\theta\hat{\sigma}_y \tag{3.6}$$

We observed that prefactors in the measurement settings did not affect the nonlocality. In other words the settings $(\cos\theta\hat{\sigma}_x + \sin\theta\hat{\sigma}_y)$, $(\cos\theta\hat{\sigma}_x - \sin\theta\hat{\sigma}_y)$ and $(\sin\theta\hat{\sigma}_x + \cos\theta\hat{\sigma}_y)$ all produced the same nonlocality functions. Hence these three

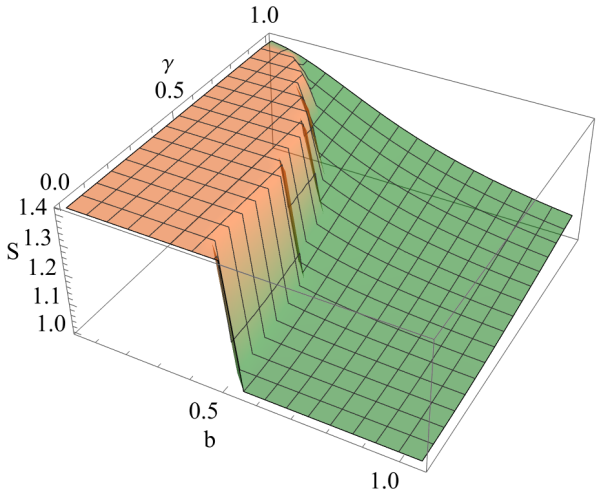

Figure 3.5: Plot of the CHSH function of the 2-spin XY chain with the $\gamma = 0$ limit corresponding to the XX model and the $\gamma = 1$ limit corresponding to the Ising model as previously analysed. The region shaded in orange indicates that measurement setting $\hat{R}^1$, $\hat{R}^2$ or $\hat{R}^3$ equally optimise the violation while the region shaded in green indicates that measurement setting $\hat{R}^2$ or $\hat{R}^3$ optimise the violation.

settings provide a sufficient variation of the possible rotations. The matrix form of the operators can be found in Appendix F.

Using these measurement settings we can compute the CHSH violation. In Figure 3.5 the CHSH violation is plotted against γ and b. We observe the limiting cases agree with previous results for the violation behaviour, as seen in Figure 2.4b and Figure 3.3b. The clear discontinuity in the CHSH function also falls along the energy level crossing in the XY model, as seen in Figure 3.4b. In the regime before the energy crossing (in orange) the violation is the constant value $\sqrt{2}$. In fact, the analytics for this regime are the same as the XX case before the energy crossing, including the values for the angles. The orange colouring indicates that any measurement settings equally optimally violates the CHSH function, while the green colouring indicates that maximal violation can be achieved by either $\hat{R}^2$ or $\hat{R}^3$. The fact that the region before the energy crossing is measurement invariant suggests that while the precise angles which optimise the violation for each observable will be different, the ultimate rotation the system undergoes to achieve maximal violation is equivalent.

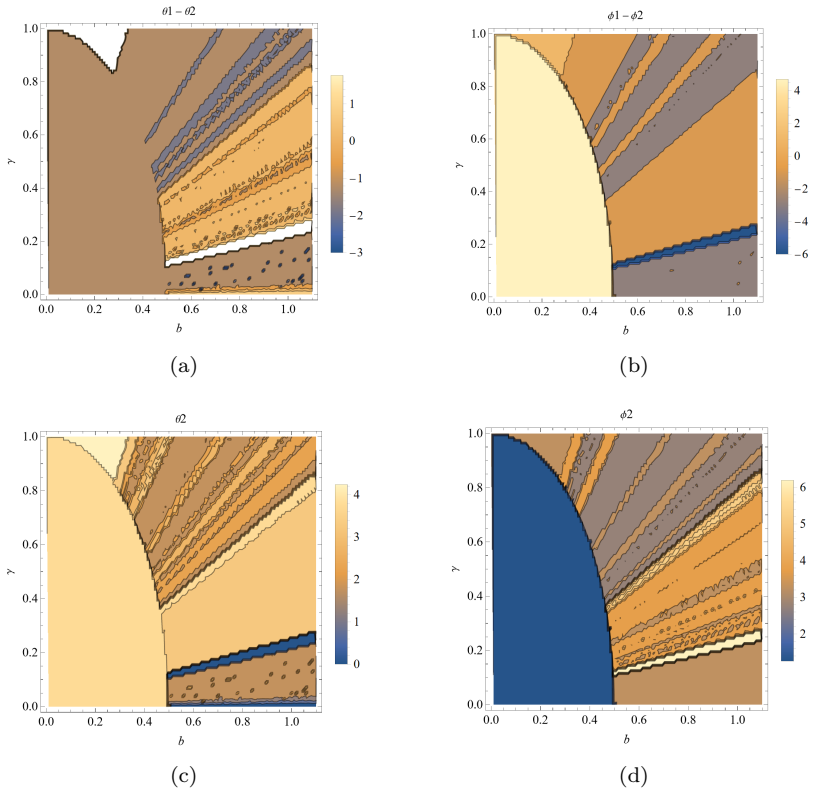

Figure 3.6: For each figure the numerical values of angle combinations are plotted against b and γ **(a)** Plot of numerical values of $\theta_1 - \theta_2$ **(b)** Plot of numerical values of $\phi_1 - \phi_2$ **(c)** Plot of numerical values of θ_2 **(d)** Plot of numerical values of ϕ_2.

In order to carry out an analysis of the angles' effect on the nonlocality in the 2-spin XY model, we only find approximations corresponding to measurement setting $\hat{R}^3$. We plot the numerical values of the angle combinations $(\theta_1 - \theta_2)$, $(\phi_1 - \phi_2)$, (θ_2) and (ϕ_2) in Figure 3.6. We can see that before the energy crossing they are constant and equivalent to the values determined for the XX model however, after the energy crossing there appear to be quite a few regions where the relationships between the angles are constant. Furthermore, the regions in which $(\theta_1 - \theta_2)$, $(\phi_1 - \phi_2)$, (θ_2) and (ϕ_2) are constant are not the same. It is clear that the angle values depend on both b and γ. Hence we will not formulate analytical approximations for the entire domain of the XY model, but will derive analytics for the specific contour $\gamma = 0.18$. When $\gamma = 0.18$, we can identify three regions where the angle relationships are approximately constant. The general form of the CHSH inequality after the energy

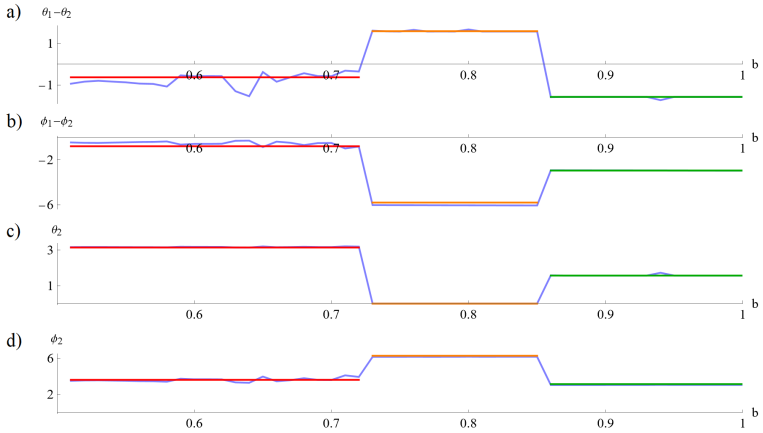

Figure 3.7: For each figure the numerical results of the angle values are plotted in blue, the analytical estimate in region one is plotted in red, the analytical estimate in region two is plotted in orange and the analytical estimate in region three is plotted in green as a function of b **(a)** Plot of numerical values of $(\theta_1 - \theta_2)$ **(b)** Plot of numerical values of $(\phi_1 - \phi_2)$ **(c)** Plot of numerical values of (θ_2) **(d)** Plot of numerical values of (ϕ_2).

level crossing in the XY model is given in Appendix G. From Figure 3.7 we can determine values of the constant angle relationships, given in Appendix H.

Substituting these values into the general CHSH function of the 2-spin XY model after the energy crossing, we produce analytical approximations for each of the 3 regions. The analytical expressions all share the same functional form with a $g/\sqrt{4b^2+g^2}$ dependence plus some constant.

$$\text{CHSH} = \begin{cases} \dfrac{0.224242g}{\sqrt{4b^2+g^2}} + 0.945322 & \text{(Region 1)} \\ \dfrac{0.226967g}{\sqrt{4b^2+g^2}} + 0.946359 & \text{(Region 2)} \\ \dfrac{0.0936907g}{\sqrt{4b^2+g^2}} + 0.991144 & \text{(Region 3)} \end{cases} \tag{3.7}$$

We can thus compare the analytical approximations to the numerical evaluation of the CHSH function, as shown in Figure 3.8. It is clear to see the analytical approximations are inadequate compared to the numerical violation. The approximation in Region 1 and Region 2 is considerably worse than the approximation in Region

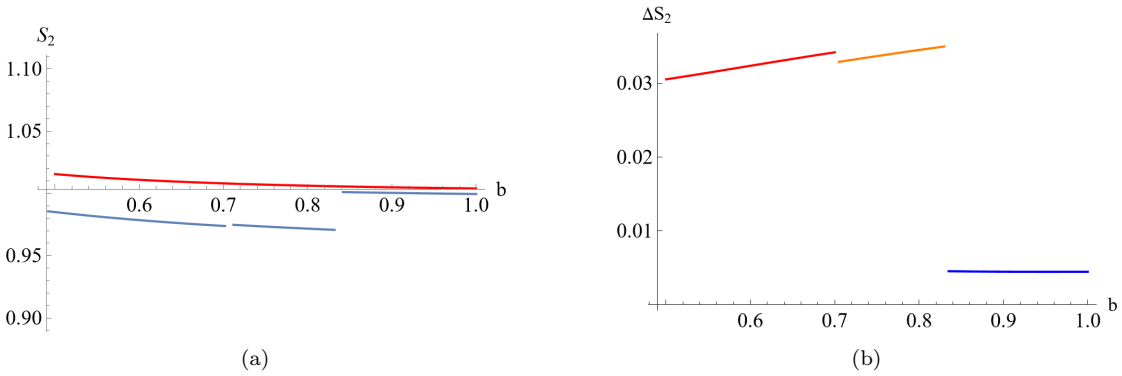

(a) (b)

Figure 3.8: **(a)** Plot comparing the numerical Svetlichny function (red) against the analytical approximations for regions one, two and three (blue) **(b)** Plot showing the error on the analytical estimates for regions one (red), two (orange) and three (blue).

3, but nevertheless none of the approximations coincide with the numerical result even once. We do note that the angle relation $(\theta_1 - \theta_2)$ in the XY case appears to be much less consistent than the corresponding relationship in the Ising limit as seen in Figure 3.1, which may explain why the analytical approximation is much worse. As it is clear that the nonlocality is quite sensitive to changes in the angles, it stands to reason the coarse approximation of $(\theta_1 - \theta_2) \simeq -\pi/5$ would introduce substantial error into the computation of the nonlocality. As such, we will proceed with a numerical-only analysis of larger system sizes.

3.2 3 Particles

Now we can extend our results to 3-particle spin chains, using the same Hamiltonian as previously, from Equation 3.1. We begin by examining the energy spectra of the Ising and XX limits, shown in Figure 3.9. As we are only interested in the zero temperature limits, we focus on the energy level crossings observed in the ground state, specifically at $b = 1$ in the XX limit. There is a degeneracy in the Ising ground state at $b = 0$, where six states coincide. We find the analytical expressions of the ground states for the Ising and XX model. The ground state for the Ising chain is strictly for $b > 0$, as at precisely $b = 0$ the ground state is a

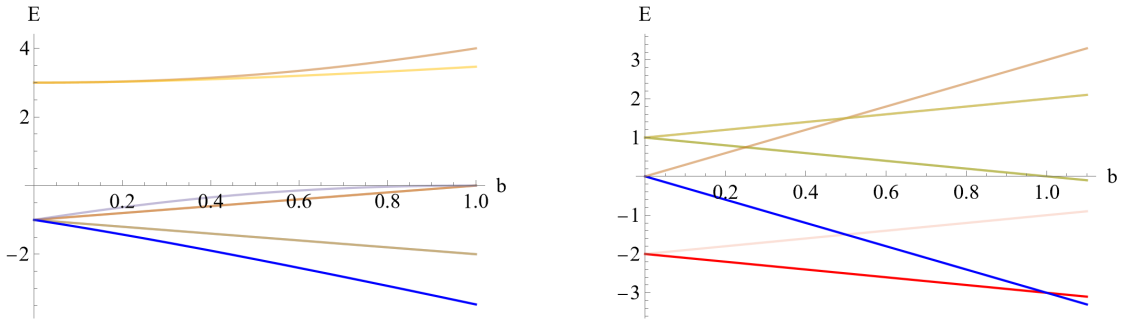

(a) (b)

Figure 3.9: **(a)** Energy spectrum for the 3-spin Ising chain as a function of b. The ground state is plotted in blue **(b)** Energy spectrum for the 3-spin XX chain as a function of b. The ground state is plotted before the energy level crossing at $b = 0.5$ (red) and after the crossing (blue).

superposition of the six degenerate eigenstates. Similar to the 2-spin chains, the XX ground state is a W-type state before the energy level crossing at $b = 1$ while afterwards it is the completely separable state $|000\rangle$.

$$|\Psi_{GS}^{\text{Ising}}\rangle = |011\rangle + |110\rangle - (1 + 2b + 2\sqrt{b^2 + b + 1}|000\rangle) + |010\rangle \qquad b > 0 \tag{3.8}$$

$$|\Psi_{GS}^{\text{XX}}\rangle = \begin{cases} \frac{1}{\sqrt{6}}|100\rangle + \frac{1}{\sqrt{6}}|010\rangle - \sqrt{\frac{2}{3}}|001\rangle & b \leq 1 \\ |000\rangle & b > 1 \end{cases} \tag{3.9}$$

A similar energy level crossing to the 2-spin XY chain appears in the 3-spin XY energy spectrum, as seen in Figure 3.10a. Here the excited energies are shaded in blue, as we are primarily interested in the ground state level crossing. The crossing has the limiting values of $(b, \gamma) = (1, 0)$ and $(b, \gamma) = (0, 1)$ corresponding to the observed degeneracies in the XX and Ising chains respectively. We can similarly find the analytical expression of the energy level crossing in the 3-spin XY chain,

$$b^* = \sqrt{1 - \gamma^2} \tag{3.10}$$

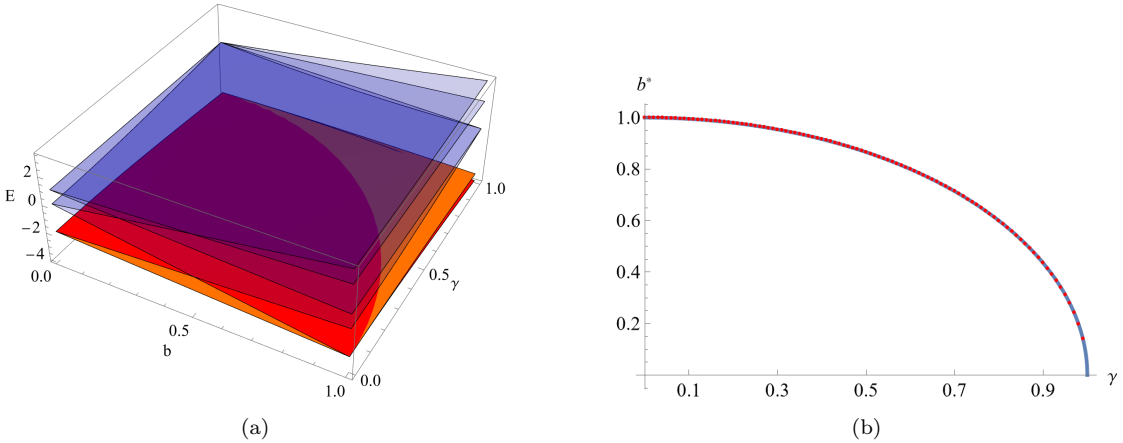

(a) (b)

Figure 3.10: **(a)** Energy spectrum of the 3-spin XY chain. There is an energy level crossing beginning at $b^* = 1$ in the XX limit and ending at $b^* = 0$ in the Ising limit **(b)** Plot of the numerical values of b^* where the energy level crossing occurs (red, dotted) against the analytical expression (blue, solid).

We analyse the Svetlichny functions in the XX and Ising limits as a function of the magnetic field, as seen in Figure 3.11. In the XX limit we can observe a step-function like behaviour, where the maximal violation of $S_3 = S_W^*$ is achieved before the energy crossing. After which, the state is completely local. As we know the XX limit is a W-type state for $b \leq 1$ from Equation 3.9, the upper bound of its violation being equivalent to the W-type upper bound is expected. It is similarly expected that there is no violation for $b > 1$ as the XX limit becomes the $|000\rangle$ state. In the Ising limit we observe similar behaviour to that of the 2-particle case, discussed in Section 2.3 and Section 3.1. Finally we can observe

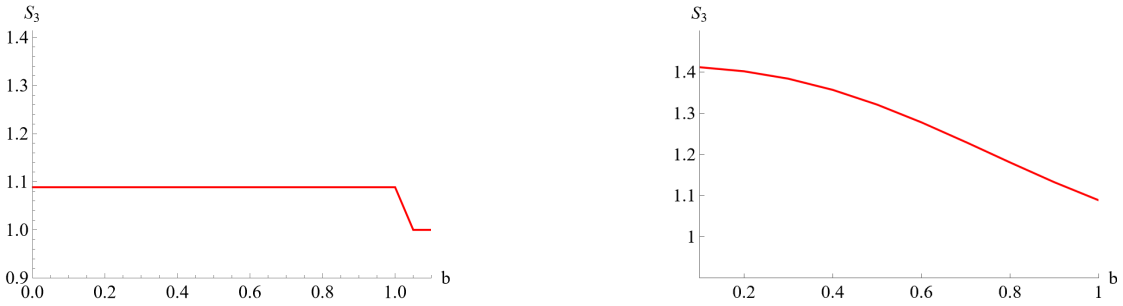

(a) (b)

Figure 3.11: **(a)** Plot of the 3-spin XX chain Svetlichny function. The maximal violation obtained is S_W^* **(b)** Plot of the 3-spin Ising chain Svetlichny function. The maximal violation obtained is $\sqrt{2}$.

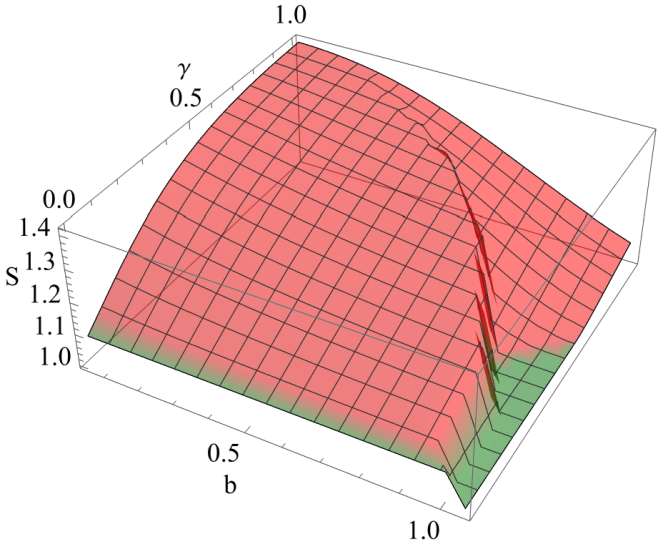

Figure 3.12: Plot of the Svetlichny violation for the 3-spin XY model against varying b and γ. In the limits of the XX and Ising model, when $\gamma = 0$ and $\gamma = 1$ respectively, maximal violations of S_W^* and $\sqrt{2}$ are obtained. The region shaded in red indicates that measurement setting $\hat{R}^3$ optimises the violation while the region shaded in green indicates that measurement setting $\hat{R}^2$ or $\hat{R}^3$ optimise the violation.

both these limits in the full Svetlichny function of the XY model, as shown in Figure 3.12. There is a clear discontinuity in the Svetlichny function along the energy level crossing. Notably before the energy crossing the Svetlichny violation is a monotone increasing function from the maximal XX bound up to the maximal Ising bound, $S_W^* \leq S_3 \leq \sqrt{2}$. As discussed in Section 2.2, we can deduce that the correlation structure in the XY regime before the energy level crossing must be a GHZ-type state. Hence we conclude that in both the Ising and XY regimes we have GHZ-type correlations whereas in the XX regime we have W-type correlations. We also perform the same analysis of the measurement settings as carried out for the 2-spin case, where the violation for each of the measurement settings laid out in Equation 3.6 was compared. The regions shaded in red indicate that measurement setting $\hat{R}^3$ maximally violated the Svetlichny function while the regions shaded in green indicate that measurement setting $\hat{R}^2$ and $\hat{R}^3$ equally maximally violate the inequality.

Hence there appears to be some congruity between the measurement settings and

correlation structure observed for the three models, where the optimal parameters overlap for the Ising and XY regimes while the XX regime has different values. While this could be a coincidence, it is worth noting that the Ising and XY models belong to the same universality class in statistical mechanics [41]. These groups are used to characterise systems with the same asymptotic behaviour in the thermodynamic limit, i.e. they share the same critical exponents. However the finite scale behaviour is *not* necessarily similar, hence we do not argue that the specifics of the large limit dynamics are of use here. Rather we are interested in the fact that the Ising model is somehow more "related" to the XY model than the XX model and also happens to share similar parameter settings. Whether this is coincidence or due to actual properties of the universality class is for further investigation.

3.3 4 Particles

Before analysing the 4-particle XY spin chain, we note that there exist nine correlation structures for four particle systems [42]. As we analysed the 3-spin chains with reference to the W and GHZ-type correlations, we will also reference the correlation structures that we observe in the 4-spin XY model. We select two of the nine structures that are particularly relevant, written as follows,

$$\begin{aligned} G_{abcd} =& \frac{a+d}{2}\Big(|0000\rangle + |1111\rangle\Big) + \frac{a-d}{2}\Big(|0011\rangle + |1100\rangle\Big) \\ &+ \frac{b+c}{2}\Big(|0101\rangle + |1010\rangle\Big) + \frac{b-c}{2}\Big(|0110\rangle + |1001\rangle\Big) \\ L_{ab_3} =& a\Big(|0000\rangle + |1111\rangle\Big) + \frac{a+b}{2}\Big(|0101\rangle + |1010\rangle\Big) \\ &+ \frac{a-b}{2}\Big(|0110\rangle + |1001\rangle\Big) + \frac{i}{\sqrt{2}}\Big(|0001\rangle + |0010\rangle + |0111\rangle + |1011\rangle\Big) \end{aligned} \tag{3.11}$$

The G_{abcd} class is the most general family and corresponds to GHZ-like correlations. For the coefficient values ($a = b = c = d = 0$), it corresponds to two pairs of EPR-states while for ($a = 1, b = 1, c = 0, d = 0$), it attains the maximal violation of

the 4-particle Svetlichny inequality of $2\sqrt{2}$. For the choice of $(d = -a)$, the 4 qubit GHZ contribution is removed leaving behind a Dicke state [43]. The L_{ab_3} state corresponds to the 4-qubit W state when $(a = b = 0)$. We lay out the upper bounds on the Svetlichny violation observed for a specific choice of coefficient values as well as the measurement setting which optimised the violation,

$$\begin{aligned} G_{abcd}(a=1,b=1,c=0,d=0) \qquad & S^*_{\text{GHZ}} \equiv S_4 = 2.82843 \qquad \hat{R}^3 \\ G_{abcd}(a,b,c,d=-a) \qquad & S^*_{\text{Dicke}} \equiv S_4 = 2.06066 \qquad (\hat{R}^2, \hat{R}^3) \\ L_{ab_3}(a=0,b=0) \qquad & S^*_{4W} \equiv S_4 = 1.5543 \qquad (\hat{R}^2, \hat{R}^3) \end{aligned} \tag{3.12}$$

With this discussion of the correlation structures, we finally analyse the 4-spin XY chain. We begin again by examining the microscopic behaviour of the limiting cases of the Ising and XX models. In particular we can examine the energy level crossing in the ground states of their energy spectra, as seen in Figure 3.13. In the Ising limit as seen in Figure 3.13a, there a single degeneracy in the ground state at $b = 0$ similar to the previous Ising cases. In the XX limit as seen in Figure 3.13b, there are two energy level crossings at $b = \sqrt{2} - 1$ and $b = 1$ and

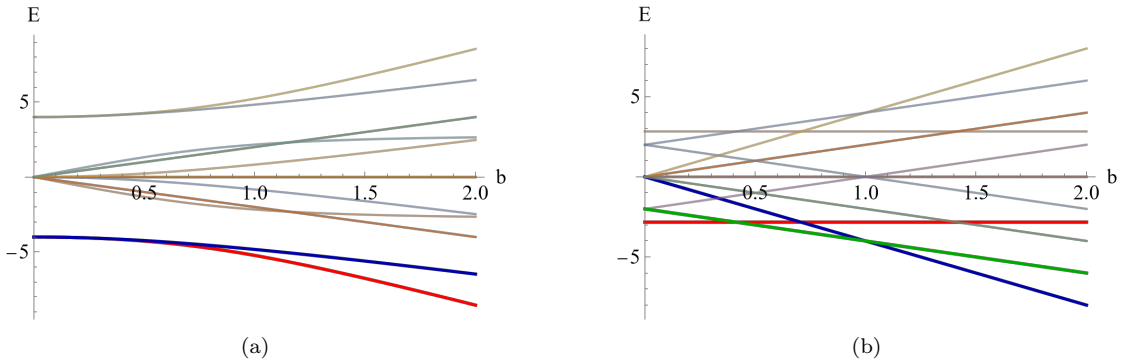

(a) (b)

Figure 3.13: **(a)** Energy spectrum for the 4-spin Ising chain as a function of b. The ground state is plotted in red and at the degeneracy $b = 0$ the ground state becomes a superposition of the blue and red energy states. The remaining curves indicate the excited energy levels **(b)** Energy spectrum for the 4-spin XX chain as a function of b. The three energy levels comprising the ground state are plotted in red, green and blue corresponding to before the first energy crossing at $b = \sqrt{2} - 1$, between the first energy crossing and the second at $b = 1$ and after the second energy crossing respectively. The remaining curves indicate the excited energy levels.

hence three different ground state expressions. For the XX limit, call the interval $0 \leq b \leq \sqrt{2}-1$ "region 1", the interval $\sqrt{2}-1 \leq b \leq 1$ "region 2" and the interval $b \geq 1$ "region 3".

The new analytical expressions for the ground states of the XX and Ising limits are shown in Equation 3.13 and Equation 3.14. We can see in region 2 the XX ground state is a W-type state, while in region 3 it is the familiar $|0000\rangle$ state. In the Ising limit we have the linear combination of a GHZ-like state with a Dicke state, which shares the same structure as a G_{abcd} state. The definitions of the coefficients are given in Appendix I. At precisely $b = 0$ the ground state becomes a superposition of the degenerate first excited state.

$$|\Psi_{GS}^{\mathrm{XX}}\rangle = \begin{cases} \frac{1}{2\sqrt{2}}\Big(|0011\rangle - |0101\rangle + |0110\rangle \\ \qquad + |1001\rangle - |1010\rangle + |1100\rangle\Big) & 0 \leq b \leq \sqrt{2}-1 \\ \frac{1}{2}\Big(-|1000\rangle + |0100\rangle - |0010\rangle + |0001\rangle\Big) & \sqrt{2}-1 \leq b \leq 1 \\ |0000\rangle & b \geq 1 \end{cases} \tag{3.13}$$

$$|\Psi_{GS}^{\mathrm{Ising}}\rangle = A|0000\rangle + B|0011\rangle + C|0101\rangle + D|0110\rangle + E|1001\rangle + F|1010\rangle + G|1100\rangle + |1111\rangle \qquad b > 0 \tag{3.14}$$

We can examine the Svetlichny violation in the Ising and XX limiting cases, as seen in Figure 3.14. Now the Svetlichny function in the XX case is a step function

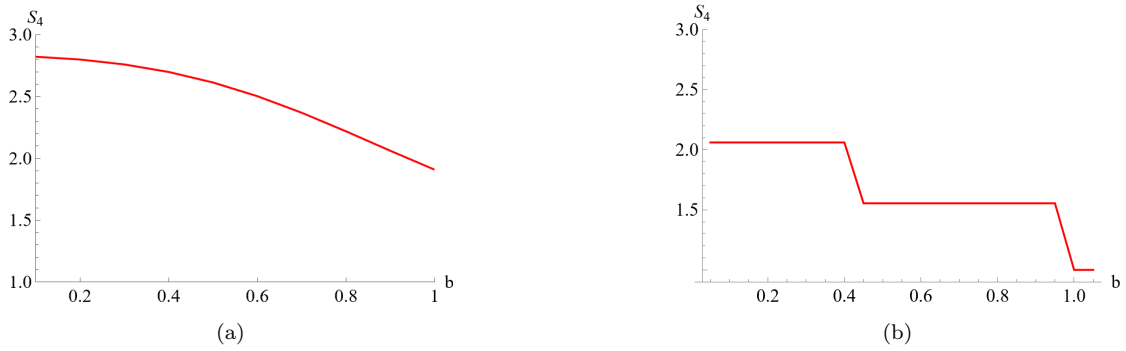

Figure 3.14: **(a)** Plot of the 4-spin Ising chain Svetlichny function. The maximal violation obtained is S^*_{GHZ} **(b)** Plot of the 4-spin XX chain Svetlichny function. The maximal violation obtained is S^*_{Dicke} in region 1, S^*_{4W} in region 2 and 1 in region 3.

with constant values in between the energy level crossings of 2.06066 in region 1, 1.5543 in region 2 and 1 in region 3. We note that these are in fact upper bounds that correspond with S^*_{Dicke} and S^*_{4W}, as defined above. Checking the functional form of the states, we can confirm that in region 1 the XX limit is a subset of the G_{abcd} class, i.e. a Dicke state, while in region 2 the XX limit is a L_{ab_3} type state, i.e. a 4-spin W state. In the Ising limit, we see a maximal violation of $2\sqrt{2} = 2.82843$, which corresponds to the upper bound S^*_{GHZ}. Again observing the functional form, we can confirm it is a part of the general G_{abcd} class, which corresponds to GHZ-like correlations.

Finally, we analyse the 4-spin Svetlichny function for the XY chain, as shown in Figure 3.15. Again we see the limiting cases obey the S_4 functions we already found for the XX and Ising model as shown in Figure 3.14a and Figure 3.14b. Now there appear two discontinuities in the Svetlichny function which are the energy level crossings corresponding to both the curves in Equation 3.5 and Equation 3.10.

Before the first energy crossing the Svetlichny violation is a monotone increasing

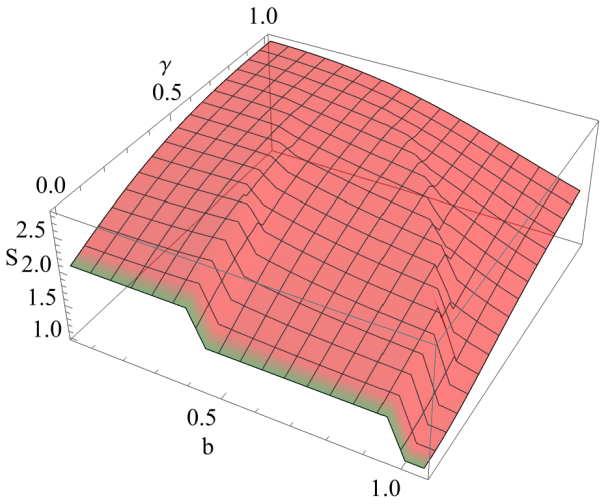

Figure 3.15: Plot of the Svetlichny function for the 4-spin XY model against varying b and γ. In the limits of the XX and Ising model the maximal violations obtained are (S^*_{Dicke},S^*_{4W},1) and S^*_{GHZ} respectively. The region shaded in red indicates that measurement setting $\hat{R}^3$ optimises the violation while the region shaded in green indicates that measurement setting $\hat{R}^2$ or $\hat{R}^3$ optimise the violation.

function from the maximal violation S^*_{Dicke}, up to the maximal violation of S^*_{GHZ} in the Ising limit. Similarly, between the first and second energy level crossing the Svetlichny violation is monotone increasing from the maximal violation S^*_{4W} up to S^*_{GHZ} (remembering that all energy level crossings coincide at the degeneracy $b = 0$ in the Ising limit). Unfortunately, as the 4-spin system is more complex than the 3-spin case with overlapping upper bounds between its various correlation structures, we cannot unequivocally determine which regions of the XY model correspond to which of the nine correlation structures. However, if we extended the 3-spin observation that the same correlation structure is shared in the XY and Ising limit, we hypothesize the 4-spin XY is of the G_{abcd} class. As we do not investigate this hypothesis in this report, we leave it for future investigation.

Lastly we computed the violation for each measurement setting in Equation 3.6. The region in red indicates $\hat{R}^3$ optimised the violation while the region in green indicates either $\hat{R}^2$ or $\hat{R}^3$ equally optimised the violation. We note that before the second energy crossing in the XY model, these are the same optimal measurement settings as observed in the 3-spin case. We also note that the optimal measurement settings for the G_{abcd} state for the choice $(a = 1, b = 1, c = 0, d = 0)$ corresponds to the Ising and XY setting, further suggesting they share the same correlation class. Similarly, the two types of correlation in the XX limit, G_{abcd} for $(d = -a)$ and L_{ab_3} for $(a = b = 0)$, share the same measurement settings as observed. From this 4-spin analysis, we conclude there are some surprising similarities to the 3-spin case.

Chapter 4

Conclusion

We have thus analysed the effect of measurement settings and system size on the observed nonlocality in 1D interacting spin chains. We demonstrated that the observed nonlocality in the 1D 2-spin Ising chain is angle-dependent and furthermore, it is quite sensitive to changes to the angle values. In particular, approximations to the angle values must be within and error of 10^{-3} in order to remain accurate to an approximate magnitude of 10^{-4}. Furthermore, the angles do not remain well-behaved throughout the parameter space of b, as we could not derive an analytical estimate for values in the interval $0.56 \leq b \leq 0.64$. We performed a similar analysis for the 1D 2-spin XX chain, showing that it is a Bell-state before an energy level crossing at $b = 0.5$ and completely separable for $b > 0.5$. This allowed us to precisely determine the angle values in the CHSH function. We also carried out an analysis of the violation in the 1D 2-spin XY chain, including an analysis of its dependency on the observables (which were selected as combinations of the Pauli spin matrices) and angles. We found that before its energy level crossing it shared the same violation as the XX limit and was measurement-invariant in this region. After its energy level crossing we found two measurement settings $\hat{R}^2$ and $\hat{R}^3$ equally optimised the violation. We found the behaviour of the angle

relationships was much less predictable for the XY chain. As such, an analytical approximation was only conducted for the $\gamma = 0.18$ contour, where there seemed to be three regions of constant behaviour. The resulting approximation had an even larger error compared to the Ising case. We did note that there was a larger variation in $(\theta_1 - \theta_2)$ compared to the Ising model which could explain the worse fit. We concluded that an analytical analysis would not have any advantages over a numerical analysis in terms of reduction of complexity and would retain a substantially large error.

For the 3-particle chain we analysed the Ising and XX limits. At this system size two correlation structures emerge - the W and GHZ types. We showed that the Ising ground state is some rotated form of a GHZ state while the XX ground state is a W state before the energy crossing and the tripartite extension of the separable state observed in the 2-spin case. In the XY regime there is also an energy crossing and we find an analytical expression of the b^* value at which it occurs. In the XX limit the maximal violation attained is S_W^* while in the Ising limit the maximal violation is $\sqrt{2}$. We deduce before the energy crossing in the XY regime the state must therefore be a GHZ-type. In addition, the same three measurement settings were compared. Setting $\hat{R}^3$ was found to optimise the violation for both the Ising and XY regions while either $\hat{R}^2$ or $\hat{R}^3$ were found to optimise the XX violation. We noted that the Ising and XY chains share the same measurement setting while the XX chain permits a slightly different configuration and comment on the potential connection this has to the Ising and XY models' shared universality class.

Finally we analysed the 4 particle chain, showing that there are now two energy level crossing in both the XX and XY chains. We laid out two of the nine possible correlation structures in 4 particle systems and compared them against the expressions found for the ground states of the Ising and XX chains. In particular we find the G_{abcd} type state maximally violates the 4-particle Svetlichny inequality, while

the L_{ab_3} type state is the 4-qubit W state. We see that the ground state Ising chain is a G_{abcd} type state for the coefficient choice $(a = 1, b = 1, c = 0, d = 0)$, which attains maximal violation of the 4-particle Svetlichny inequality, S^*_{GHZ}. The XX ground state is seen to be a Dicke state, which is subset of the G_{abcd} class for the coefficient choice $(d = -a)$, for $0 \leq b \leq \sqrt{2} - 1$, a 4-spin W state for $\sqrt{2} - 1 \leq b \leq 1$ and the separable $|0000\rangle$ state for $b \geq 1$. Lastly we analysed the same measurement settings for the 4-spin case and recognised they shared the same configuration as the 3-spin case. This configuration was also found to optimise the violation for the corresponding $G_{abcd}(a = 1, b = 1, c = 0, d = 0)$, $G_{abcd}(d = -a)$ and L_{ab_3} structures.

The patterns observed between the 3-spin and 4-spin cases suggest some sort of connection between the measurement settings and either the universality classes or correlation structures of the models, which is left for further study. As this project set out to investigate the effects of the microscopic description on nonlocality, many of the specific parameters we analysed, such as the choice of spin chain model, measurement settings and system size, can be changed and re-examined. For example, the $\Delta \neq 0$ case for the general Hamiltonian we defined could be analysed, which would describe the XXZ model [44]. For four or more particles, long-range interactions between the spins could be considered as in the LMG model [45], as we only considered nearest-neighbour interactions. Similar to the 1D Ising model results we replicated, analysis could be performed for the thermal XX and XY chain to see whether we observe similar behaviour [40]. We also only examined 1D spin chains with qubits, however some literature has established tools in the way of d-dimensional systems [46]. Finally, the full range of possible correlation structures is not known for 5-particle systems and is not predictable from smaller system sizes, leaving it an open question in the literature.

Appendix

A QMI for a 2-Qubit Werner State

$$\mathrm{QMI}_{\mathrm{Werner}}(p) = \frac{(3p+1)\log(3p+1) - 3(p-1)\log(1-p)}{\log 16}$$

B EF for a 2-Qubit Werner State

$$\begin{aligned} E_F(p) =& \frac{1}{\log 16}\Bigg[\left(\sqrt{-9p^2+6p+3}-2\right)\log\left(\frac{1}{4}\left(2-\sqrt{-9p^2+6p+3}\right)\right) \\ & - \left(\sqrt{-9p^2+6p+3}+2\right)\log\left(\frac{1}{4}\sqrt{-9p^2+6p+3}+2\right)\Bigg] \end{aligned}$$

C Analytical Approximations for the 2-Spin Ising Chain Angles

$$\mathrm{R1} = \begin{cases} \theta_1 - \theta_2 = \pi/2 \\ \phi_1 - \phi_2 = 3\pi/2 \\ \theta_2 + \phi_2 = \pi/4 \\ \theta_2 - \phi_2 = -\pi/8 \end{cases} \qquad \mathrm{R2} = \begin{cases} \theta_1 - \theta_2 = -\pi/4 \\ \phi_1 - \phi_2 = -5\pi/4 \\ \theta_2 + \phi_2 = 3\pi/2 \\ \theta_2 - \phi_2 = -\pi \end{cases}$$

D General CHSH Function for the Ground State 2-Spin Ising Chain

$$S_2 = \frac{1}{2}\Bigg(\sin\theta_2 \left(\sin\phi_1 - \sin\phi_2\right) + \sin\theta_1 \left(\sin\phi_1 + \sin\phi_2\right) - \frac{1}{\sqrt{4b^2+1}}\Big(\cos\theta_2 \left(\cos\phi_1 - \cos\phi_2\right) + \cos\theta_1 \left(\cos\phi_1 + \cos\phi_2\right) \Big) \Bigg)$$

E Optimal Angles for 2-spin Ising chain CHSH Inequality

$$b \leq 0.5 \begin{cases} \theta_1 = 2.04817 \\ \theta_2 = 3.61897 \\ \phi_1 = 5.97516 \\ \phi_2 = 1.26277 \end{cases} \qquad b > 0.5 \begin{cases} \theta_1 = 0 \\ \theta_2 = 0.01867 \\ \phi_1 = 0 \\ \phi_2 = \pi \end{cases}$$

F Matrix Form of Measurement Settings

$$\hat{R}^1 = \begin{pmatrix} 0 & \cos\theta - i\sin\theta \\ \cos\theta + i\sin\theta & 0 \end{pmatrix}$$

$$\hat{R}^2 = \begin{pmatrix} \sin\theta & \cos\theta \\ \cos\theta & -\sin\theta \end{pmatrix} \quad \hat{R}^3 = \begin{pmatrix} \cos\theta & -i\sin\theta \\ i\sin\theta & -\cos\theta \end{pmatrix}$$

G General CHSH Function for the Ground State 2-Spin XY Chain

$$S_2 = \frac{1}{2}\Bigg(\cos\theta_1 \left(\cos\phi_1 - \cos\phi_2\right) + \cos\theta_2 \left(\cos\phi_1 + \cos\phi_2\right) + \frac{g}{\sqrt{4b^2+g^2}}\Big(\sin\theta_1 \left(\sin\phi_1 - \sin\phi_2\right) + \sin\theta_2 \left(\sin\phi_1 + \sin\phi_2\right) \Big) \Bigg)$$

H Analytical Approximations for the 2-Spin XY Chain Angles

$$\text{R1} = \begin{cases} \theta_1 - \theta_2 = -\frac{\pi}{5} \\ \phi_1 - \phi_2 = -\frac{\pi}{4} \\ \theta_2 = \pi \\ \phi_2 = \frac{23}{20}\pi \end{cases} \qquad \text{R2} = \begin{cases} \theta_1 - \theta_2 = \pi/2 \\ \phi_1 - \phi_2 = -\frac{37}{20}\pi \\ \theta_2 = 0 \\ \phi_2 = 2\pi \end{cases} \qquad \text{R3} = \begin{cases} \theta_1 - \theta_2 = -\frac{\pi}{2} \\ \phi_1 - \phi_2 = -\frac{47}{50}\pi \\ \theta_2 = \frac{\pi}{2} \\ \phi_2 = \pi \end{cases}$$

I Coefficients of the 4-Spin Ground State Ising Expression

$$A = 2\sqrt{b^4+1} + 2b^2 + \sqrt{2}\sqrt{\sqrt{b^4+1}+b^2+1}\,b + \frac{\sqrt{2}}{b}\left(\sqrt{\left(b^4+1\right)\left(\sqrt{b^4+1}+b^2+1\right)} - \sqrt{\sqrt{b^4+1}+b^2+1}\right) - 1$$

$$B = -\frac{\sqrt{\sqrt{b^4+1}+b^2+1}}{\sqrt{2}} - b \qquad E = -\frac{\sqrt{\sqrt{b^4+1}+b^2+1}}{\sqrt{2}} - b$$

$$C = \frac{\sqrt{2}b}{\sqrt{\sqrt{b^4+1}+b^2+1}} + 1 \qquad F = \frac{\sqrt{2}b}{\sqrt{\sqrt{b^4+1}+b^2+1}} + 1$$

$$D = -\frac{\sqrt{\sqrt{b^4+1}+b^2+1}}{\sqrt{2}} - b \qquad G = -\frac{\sqrt{\sqrt{b^4+1}+b^2+1}}{\sqrt{2}} - b$$

Bibliography

[1] Christian L Degen, Friedemann Reinhard, and Paola Cappellaro. Quantum sensing. *Reviews of modern physics*, 89(3):035002, 2017.

[2] Valerio Scarani, Helle Bechmann-Pasquinucci, Nicolas J Cerf, Miloslav Dušek, Norbert Lütkenhaus, and Momtchil Peev. The security of practical quantum key distribution. *Reviews of modern physics*, 81(3):1301, 2009.

[3] Iulia M Georgescu, Sahel Ashhab, and Franco Nori. Quantum simulation. *Reviews of Modern Physics*, 86(1):153, 2014.

[4] John Goold, Marcus Huber, Arnau Riera, Lídia Del Rio, and Paul Skrzypczyk. The role of quantum information in thermodynamics—a topical review. *Journal of Physics A: Mathematical and Theoretical*, 49(14):143001, 2016.

[5] Albert Einstein, Boris Podolsky, and Nathan Rosen. Can quantum-mechanical description of physical reality be considered complete? *Physical review*, 47(10):777, 1935.

[6] David Bohm. A suggested interpretation of the quantum theory in terms of "hidden" variables. i. *Physical review*, 85(2):166, 1952.

[7] John S Bell. On the einstein podolsky rosen paradox. *Physics Physique Fizika*, 1(3):195, 1964.

[8] Thomas Young. I. the bakerian lecture. experiments and calculations relative to physical optics. *Philosophical transactions of the Royal Society of London*, (94):1–16, 1804.

[9] Niels Bohr. Essays 1958-1962 on atomic physics and human knowledge. 1963.

[10] John Bell. Against 'measurement'. *Physics world*, 3(8):33, 1990.

[11] Jan-Åke Larsson. Loopholes in bell inequality tests of local realism. *Journal of Physics A: Mathematical and Theoretical*, 47(42):424003, 2014.

[12] Daniel Cavalcanti, Mafalda L Almeida, Valerio Scarani, and Antonio Acin. Quantum networks reveal quantum nonlocality. *Nature communications*, 2(1):184, 2011.

[13] Alessia Suprano, Davide Poderini, Emanuele Polino, Iris Agresti, Gonzalo Carvacho, Askery Canabarro, Elie Wolfe, Rafael Chaves, and Fabio Sciarrino. Experimental genuine tripartite nonlocality in a quantum triangle network. *PRX Quantum*, 3(3):030342, 2022.

[14] Lars Onsager. Crystal statistics. i. a two-dimensional model with an order-disorder transition. *Physical Review*, 65(3-4):117, 1944.

[15] Adeline Orieux, Joelle Boutari, Marco Barbieri, Mauro Paternostro, and Paolo Mataloni. Experimental linear-optics simulation of multipartite nonlocality in the ground state of a quantum ising ring. *Scientific Reports*, 4(1):1–6, 2014.

[16] Tobias Schätz, Axel Friedenauer, Hector Schmitz, Lutz Petersen, and Steffen Kahra. Towards (scalable) quantum simulations in ion traps. *Journal of Modern Optics*, 54(16-17):2317–2325, 2007.

[17] Antoni Wójcik, Tomasz Łuczak, Paweł Kurzyński, Andrzej Grudka, Tomasz Gdala, and Małgorzata Bednarska. Unmodulated spin chains as universal

quantum wires. *Physical Review A*, 72(3):034303, 2005.

[18] Rodney J Baxter. *Exactly solved models in statistical mechanics*. Elsevier, 2016.

[19] Michael A Nielsen and Isaac Chuang. Quantum computation and quantum information, 2002.

[20] John F Clauser, Michael A Horne, Abner Shimony, and Richard A Holt. Proposed experiment to test local hidden-variable theories. *Physical review letters*, 23(15):880, 1969.

[21] Alain Aspect, Philippe Grangier, and Gérard Roger. Experimental realization of einstein-podolsky-rosen-bohm gedankenexperiment: a new violation of bell's inequalities. *Physical review letters*, 49(2):91, 1982.

[22] Stuart J Freedman and John F Clauser. Experimental test of local hidden-variable theories. *Physical Review Letters*, 28(14):938, 1972.

[23] Philip M Pearle. Hidden-variable example based upon data rejection. *Physical Review D*, 2(8):1418, 1970.

[24] John Stewart Bell. Atomic-cascade photons and quantum-mechanical nonlocality. In *Quantum Mechanics, High Energy Physics And Accelerators: Selected Papers Of John S Bell (With Commentary)*, pages 782–787. World Scientific, 1995.

[25] J-Å Larsson and Richard David Gill. Bell's inequality and the coincidence-time loophole. *Europhysics letters*, 67(5):707, 2004.

[26] Jonathan Barrett, Daniel Collins, Lucien Hardy, Adrian Kent, and Sandu Popescu. Quantum nonlocality, bell inequalities, and the memory loophole. *Physical Review A*, 66(4):042111, 2002.

[27] Gregor Weihs, Thomas Jennewein, Christoph Simon, Harald Weinfurter, and Anton Zeilinger. Violation of bell's inequality under strict einstein locality conditions. *Physical Review Letters*, 81(23):5039, 1998.

[28] Bas Hensen, Hannes Bernien, Anaïs E Dréau, Andreas Reiserer, Norbert Kalb, Machiel S Blok, Just Ruitenberg, Raymond FL Vermeulen, Raymond N Schouten, Carlos Abellán, et al. Loophole-free bell inequality violation using electron spins separated by 1.3 kilometres. *Nature*, 526(7575):682–686, 2015.

[29] Marissa Giustina, Marijn AM Versteegh, Sören Wengerowsky, Johannes Handsteiner, Armin Hochrainer, Kevin Phelan, Fabian Steinlechner, Johannes Kofler, Jan-Åke Larsson, Carlos Abellán, et al. Significant-loophole-free test of bell's theorem with entangled photons. *Physical review letters*, 115(25):250401, 2015.

[30] Lynden K Shalm, Evan Meyer-Scott, Bradley G Christensen, Peter Bierhorst, Michael A Wayne, Martin J Stevens, Thomas Gerrits, Scott Glancy, Deny R Hamel, Michael S Allman, et al. Strong loophole-free test of local realism. *Physical review letters*, 115(25):250402, 2015.

[31] George Svetlichny. Distinguishing three-body from two-body nonseparability by a bell-type inequality. *Physical Review D*, 35(10):3066, 1987.

[32] Daniel Collins, Nicolas Gisin, Sandu Popescu, David Roberts, and Valerio Scarani. Bell-type inequalities to detect true n-body nonseparability. *Physical review letters*, 88(17):170405, 2002.

[33] Steve Campbell and Mauro Paternostro. Multipartite nonlocality in a thermalized ising spin chain. *Physical Review A*, 82(4):042324, 2010.

[34] Charles H Bennett, David P DiVincenzo, John A Smolin, and William K Wootters. Mixed-state entanglement and quantum error correction. *Physical*

Review A, 54(5):3824, 1996.

[35] Pranaw Rungta, Vladimir Bužek, Carlton M Caves, Mark Hillery, and Gerard J Milburn. Universal state inversion and concurrence in arbitrary dimensions. *Physical Review A*, 64(4):042315, 2001.

[36] William K Wootters. Entanglement of formation and concurrence. *Quantum Inf. Comput.*, 1(1):27–44, 2001.

[37] Reinhard F Werner. Quantum states with einstein-podolsky-rosen correlations admitting a hidden-variable model. *Physical Review A*, 40(8):4277, 1989.

[38] Wolfgang Dür, Guifre Vidal, and J Ignacio Cirac. Three qubits can be entangled in two inequivalent ways. *Physical Review A*, 62(6):062314, 2000.

[39] Daniel M Greenberger, Michael A Horne, and Anton Zeilinger. Going beyond bell's theorem. *Bell's theorem, quantum theory and conceptions of the universe*, pages 69–72, 1989.

[40] Zhao-Yu Sun, Meng Li, Long-Hui Sheng, and Bin Guo. Multipartite nonlocality in one-dimensional quantum spin chains at finite temperatures. *Physical Review A*, 103(5):052205, 2021.

[41] Luigi Amico, Rosario Fazio, Andreas Osterloh, and Vlatko Vedral. Entanglement in many-body systems. *Reviews of modern physics*, 80(2):517, 2008.

[42] Frank Verstraete, Jeroen Dehaene, Bart De Moor, and Henri Verschelde. Four qubits can be entangled in nine different ways. *Physical Review A*, 65(5):052112, 2002.

[43] Robert H Dicke. Coherence in spontaneous radiation processes. *Physical review*, 93(1):99, 1954.

[44] L Justino and Thiago R de Oliveira. Bell inequalities and entanglement at quantum phase transitions in the xxz model. *Physical Review A*, 85(5):052128, 2012.

[45] Jia Bao, Bin Guo, Hong-Guang Cheng, Mu Zhou, Jin Fu, Yi-Chen Deng, and Zhao-Yu Sun. Multipartite nonlocality in the lipkin-meshkov-glick model. *Physical Review A*, 101(1):012110, 2020.

[46] Nicolas Brunner, Daniel Cavalcanti, Stefano Pironio, Valerio Scarani, and Stephanie Wehner. Bell nonlocality. *Reviews of modern physics*, 86(2):419, 2014.